JOURNAL OF GEOPHYSICAL RESEARCH, VOL. 97, NO. E8, PAGES 13,643–13,665 AUGUST 25, 1992

Fluid Outflows From Venus Impact Craters: Analysis From Magellan Data

PAUL D. ASIMOW[1]

Department of Earth and Planetary Sciences, Harvard University, Cambridge, Massachusetts

JOHN A. WOOD

Smithsonian Astrophysical Observatory, Cambridge, Massachusetts

Many impact craters on Venus have unusual outflow features originating in or under the continuous ejecta blankets and continuing downhill into the surrounding terrain. These features clearly resulted from flow of low-viscosity fluids, but the identity of those fluids is not clear. In particular, it should not be assumed a priori that the fluid is an impact melt. A number of candidate processes by which impact events might generate the observed features are considered, and predictions are made concerning the rheological character of flows produced by each mechanism. A sample of outflows was analyzed using Magellan images and a model of unconstrained Bingham plastic flow on inclined planes, leading to estimates of viscosity and yield strength for the flow materials. It is argued that at least two different mechanisms have produced outflows on Venus: an erosive, channel-forming process and a depositional process. The erosive fluid is probably an impact melt, but the depositional fluid may consist of fluidized solid debris, vaporized material, and/or melt.

INTRODUCTION

Recently acquired high-resolution radar images of Venus from the Magellan spacecraft have revealed surface features in unprecedented detail. In addition to new views of previously known features, a series of completely new and often enigmatic features have been discovered. Among the new phenomena observed, the character of ejecta deposits around impact craters ranks as one of the most enigmatic. In addition to the expected radial distribution of continuous ejecta, left by material ballistically ejected, there are nonradial features with a flowlike or channel-like appearance that are generally too long to be explained by any ballistic process (Figure 1) [*Phillips et al.*, 1991]. These structures will be called "crater outflow features"; this usage is meant to set them apart from continuous, radial, or ballistic ejecta, even when there is evidence of some fluidization of the main ejecta blanket. The superficial resemblance of the outflow facies of Venus impact craters to a number of flow phenomena in various environments (terrestrial, Venusian, lunar, and Martian lava flows, as well as terrestrial, Martian, and lunar debris flows, and Martian fluidized ejecta blankets; Figure 2), together with their clearly nonballistic character and their tendency to extend down topographic gradients away from their crater sources, strongly suggests that these structures result from fluid flow phenomena of some variety. The continuous ejecta blankets often display a lobate edge, suggesting some flow during or after emplacement, but the crater outflows are clearly distinct features with much higher fluidity. The present study attempts to confirm this interpretation and, more importantly, to determine the rheology of the flow materials and, if possible, to identify those materials. It should be kept in mind that the flows observed are extremely diverse in appearance and may represent more than one distinct process and/or material.

SETTING AND MORPHOLOGY OF VENUS CRATER OUTFLOW FEATURES

Over 800 impact craters were identified in images produced by the Magellan mission during its first cycle of orbital mapping, ranging in diameter from 3 km to 280 km (R.R. Herrick, personal communication, 1991). The structures beyond the rims of Venus craters can be conveniently divided into four facies, all of which are seen at crater Aurelia in Figure 3: "hummocky ejecta", "outer ejecta", "dark haloes", and crater outflow features. The hummocky ejecta and outer ejecta will be grouped hereafter under the name "continuous ejecta"; azimuthal sectors of the continuous ejecta blanket are often missing, as in Figure 3 [*Phillips et al.*, 1991]. The edge of the continuous ejecta usually has a lobate to petal-like shape suggestive of limited flow upon emplacement, probably caused by turbulent entrainment of very fine ejecta particles by the dense Venus atmosphere [*Schultz*, 1991*b*]. Crater outflow features have been detected in association with at least 100 craters to date. These outflows are distinguished from the continuous or hummocky ejecta blanket by their length, brightness signatures, nonradial distribution, complex morphology, and/or sinuous planform. Outflows are recognized most readily near craters in plains regions, but they are observed in all geologic settings, from smooth plains to the highland/tessera area Tellus Regio (Figure 4). They may extend several crater radii from the edge of the continuous ejecta, although some outflows are only a few kilometers long.

There are several modes of occurrence of outflow features. Some craters, such as Kemble (Figure 5), exhibit one narrow outflow originating from a small region at the edge of the ejecta blanket; this simple appearance is fairly rare. Many (perhaps 25%) craters have exactly two outflows associated with them. The two outflows from a given crater may originate from different points adjacent to the ejecta blanket, often nearly opposite each other in azimuth, such as at Aglaonice or Danilova (Figures 1*a*

[1] Now at Division of Geological and Planetary Sciences, California Institute of Technology, Pasadena.

Paper Number 92JE00981
0148-0227/92/92JE-00981$05.00

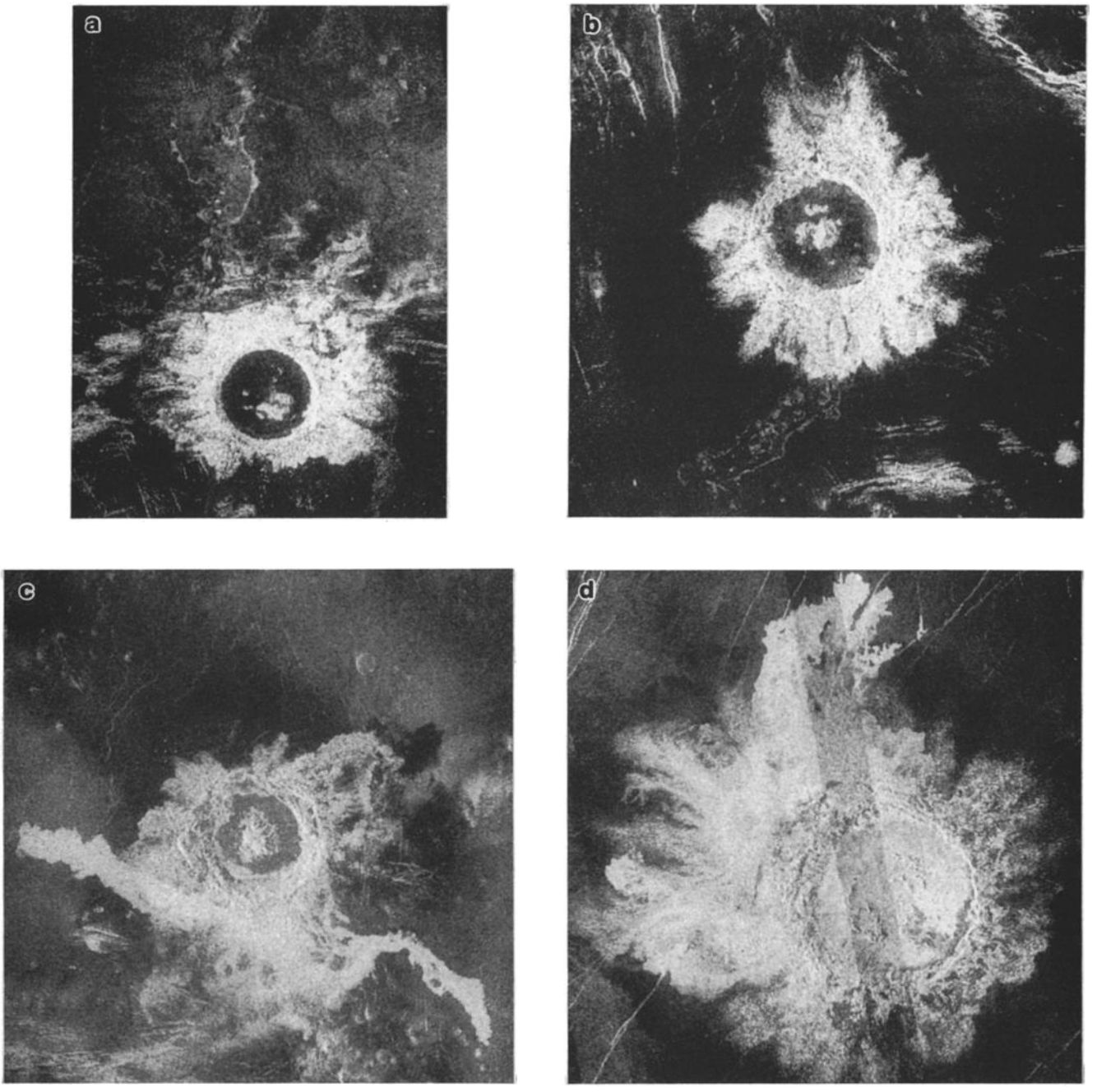

Figure 1. Full-resolution Magellan radar images of impact craters on Venus. In all Magellan radar images, north is up, and illumination is from the west. (*a*) Aglaonice (26.2°S, 339.7°E; diameter 63 km), with large fluid outflow to north and small outflow to southeast. (*b*) Danilova (26.6°S, 337.2°E; diameter 48 km), with large outflow to south and small outflow to north. (*c*) Carson (24°S, 343°E; diameter 39 km), with two bright flows originating to south and flowing to east and west. (*d*) Stuart (30°S, 21°E; diameter 67 km).

and 1*b*). They may also originate from a common area but flow in opposite directions from that point, as at Carson (Figure 1*c*) and Parra (Figure 6). Another common morphology for outflows is a broad splay, composed of multiple subflows and covering up to 180° in azimuth, such as at crater Stuart (Figure 1*d*). The development of multiple flows originating from one broad source area is quite common at smaller craters (Figure 7).

The source area of the outflows appears sometimes to be beneath the ejecta blanket and sometimes within it (compare Figures 8*a* and 8*b*). The apparent stratigraphic relationship between outflow and ejecta can be established in some but not all cases, and both relationships (outflow underlying ejecta and outflow modifying ejecta) are evident in particular cases. The edge of the continuous ejecta may appear unmodified at the source area of the flow, or it may show extensive modification: the lobate outline may be destroyed or blurred and dark linear to arcuate features subparallel to the outflow direction may appear in the outer regions of the ejecta blanket. Often, the boundary between the continuous ballistic ejecta and the outflow deposits cannot be distinguished (Figure 1*d*).

The azimuth direction of outflows is most likely determined by local topography or impact direction, the only sources of asymmetry or preferred direction. Where the radial distribution of ejecta suggests an oblique impact, single outflows sometimes

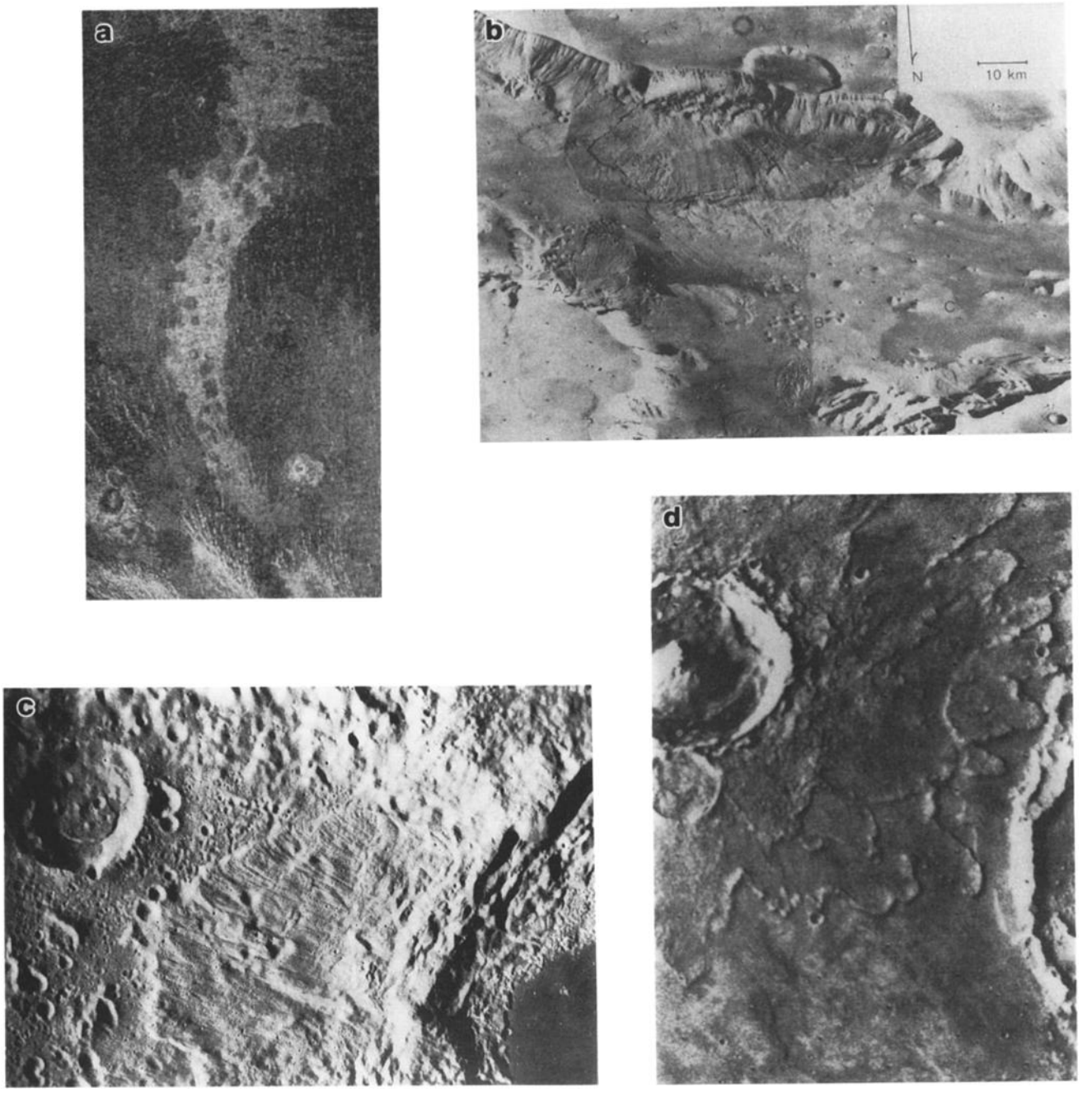

Figure 2. Examples of deposits left by flow processes. (*a*) Magellan radar image of lava flow from large volcano Sif Mons, at 7°N, 350°E. Width of frame 154 km. (*b*) Viking orbiter mosaic 14A27-32, showing large avalanche deposit from wall of Valles Marineris on Mars, extending across valley floor. Scale shown. (*c*) Apollo 17 orbiter frame M-2608, showing large avalanche deposit from rim of farside crater Tsiolkovsky. Lineated avalanche deposit is about 80 long. (*d*) Viking orbiter mosaic 3A07, showing impact crater Yuty (diameter 19 km) on Mars with characteristic fluidized ejecta blanket, including outer rampart and multiple flow lobes.

appear to have originated at the downrange point, such as at Aurelia (Figure 3). More often, the azimuths of single and multiple flows differ substantially from the apparent downrange direction, such as at Jeanne (Figure 9). In cases where two flows emerge from one crater, their directions may be generally opposite, with one flow roughly uprange and the other approximately downrange. Although the azimuth of the point of origin of the outflows and the near-source flow direction may be controlled by impact direction, the direction of subsequent flow appears to follow local topography. Thus the two outflows in Figure 6 cited above originate on the uphill/downrange side of the crater but then turn and flow downhill around the crater. The slopes down which the outflows travel are, without exception to date, very low. Slopes obtained from Magellan altimetry are somewhat uncertain (see below under Methodology), but most are virtually flat, of the order of 0.5° or lower. The detailed path of the flow may be controlled by preexisting surface structures, especially faults and grabens (e.g., Figure 10).

The morphology of the outflows themselves is highly variable. The simplest forms are uniformly bright, straight to slightly sinuous, with lobate ends (Figures 1*c* and 6). The width of the outflow is often approximately constant along its length but may

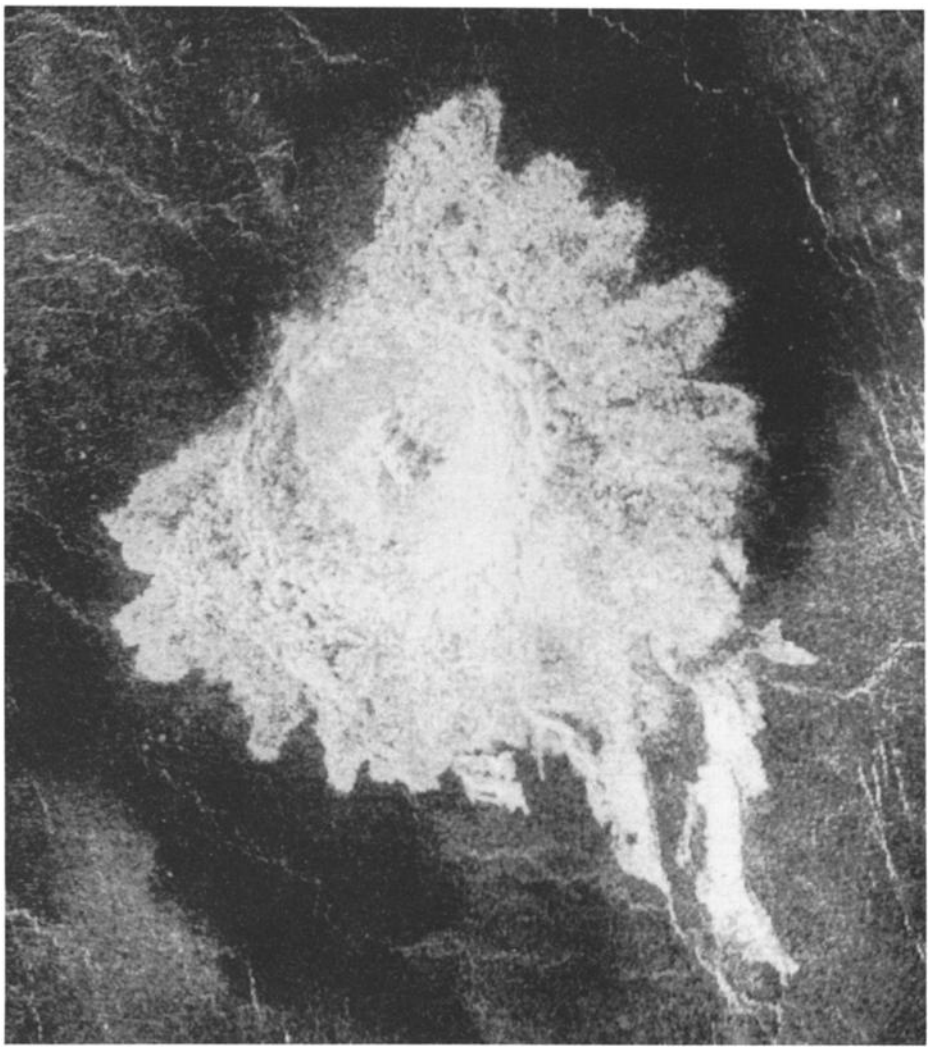

Figure 3. Magellan full-resolution radar image of crater Aurelia (20.3°N,331.8°E; diameter 31 km). Note standard elements of crater deposits on Venus: central peak, flat floor, terraced inner walls, sharp topographic rim, hummocky inner ejecta, lobate-edged outer continuous ejecta, dark halo on surrounding plains, and outflows to southeast. Note missing sector of ejecta to northwest.

increase or decrease downstream. Some flows are narrow and sinuous upstream but feed into broad fans, possibly as they cross breaks in slope. Some larger examples of simple outflows have dark interior regions and bright margins, often with bright rings around obstacles in the interior of the flow (Figure 11). It is tempting to interpret the bright margins as stationary flow levees, but this interpretation must be made carefully. At the incidence angles used by the Magellan radar system, brightness is mostly a function of surface roughness at the centimeter scale and not of topographic relief. Thus the bright margins are certainly rougher than the dark interiors, but it cannot be determined whether they are higher or lower. Most outflows take the form of multiple flow units, which may show forms analogous to braiding or anastomosing; these multiple flows are often extremely complex. Morphology similar to braiding is apparent in the small flow to the southeast of Aglaonice (Figures 1*a* and 12), whereas a more chaotic, perhaps anastamosing, regime is seen in the outflow from the 165-km crater Isabella (Figure 13).

Although the fluidized origin of crater outflow features is generally accepted [*Phillips et al.*, 1991], there are two fundamentally distinct and mutually exclusive interpretations of these structures. Some workers [*Baker et al.*, 1991; *Komatsu et al.*, 1991] categorize the crater flows as channels, resulting from an essentially erosive process. The observed outflow structures are interpreted as excavated regions, with deposition of the transported and eroded material only at their distal ends. This model assumes that the same process is responsible for crater outflows and for the various volcanic channels or rilles discovered on Venus in Magellan images. The principal item of evidence for this interpretation is the presence of eroded or streamlined remnant "islands" in midchannel (Figures 11 and 13). Baker et al. assume a priori that the flow material was a melt-rock of some variety; they do not evaluate any debris flow hypotheses. The alternative view is that crater flows are depositional features, with positive surface relief [*Phillips et al.*, 1991]. A depositional flow will display channel-like morphology in radar images if it creates stationary lateral levees.

The present study is concerned only with those flows whose character can be interpreted as depositional, although there appear to be flows created by both mechanisms: compare Figures 11 and 13. Unambiguous separation of channels from positive-relief deposits requires much higher resolution topography or high incidence angle radar images; such data may be gathered in the extended mission of the Magellan project. In the absence of

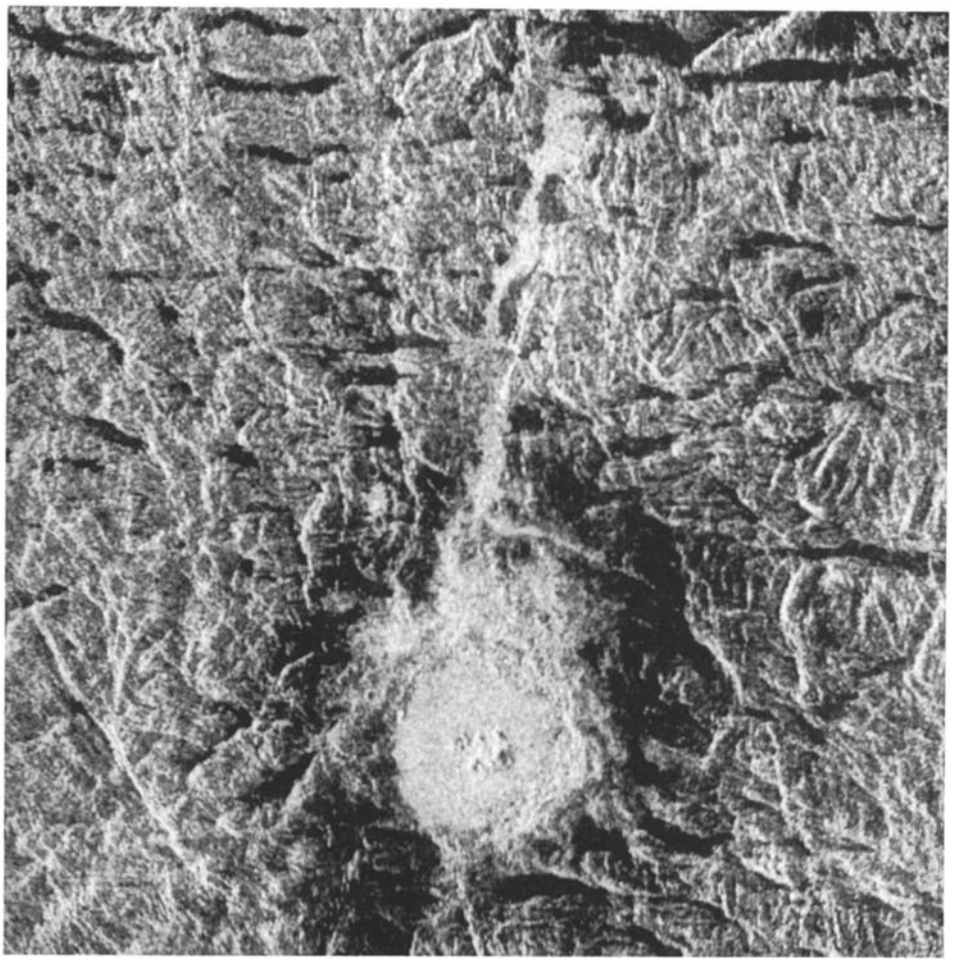

Figure 4. Crater Khatun in Tellus Regio (40°N,86°E; diameter 44 km). Magellan full-resolution radar image. Note bright outflow to north, filling valley in extremely disrupted terrain.

unambiguous data, the interpretation that many of the crater outflow features are depositional in origin is motivated by several observations: (1) the scale and gross morphology of these deposits are distinct from the channels described by *Baker et al.* [1991]. (2) The lobate planimetric form of the deposits closely resembles depositional features such as lava flows and debris flows. (3) The extraordinary width of the flows requires an extremely low cross-sectional aspect ratio (it is not possible for a channel to be several kilometers deep), which will make the assumption of unconstrained surface flow more useful in modelling the outflow process than the usual assumptions of semielliptical or semirectangular channels.(4) Erosive channels must have a "drainage region" where the fluid which excavates the channel is eventually deposited, whereas the crater outflows generally lack any such associated feature (with the notable exception of Figure 13), suggesting that the material which formed the outflows constitutes the observed deposit. (5) Assuming that crater outflows are caused by cratering events, they were most likely produced by a sudden, short-lived process, whereas the time scales for thermal erosion by lavas require continuous high-volume effusion for a significant period in order to form erosional channels. (6) The "streamlined islands" thought to represent uneroded regions between anastamosing crater outflow segments often show clear summit pits and generally circular outlines, in contrast to the genuinely streamlined islands in other channels. These are interpreted as small shield volcanoes, which are extremely common on Venus and are high enough (50 to 100 m) to stand above a depositional flow. The similarity between the "islands" in a clearly depositional lava flow from the large volcano Sif Mons (Figure 2*a*) and in some crater flows (Figure 11) is extremely strong.

MODEL AND ANALYSIS

The rheological behavior of a broad class of geological fluids is often approximated by a plastic model, first described by *Bingham* [1922], which introduces a finite yield strength S_y and a constant Bingham viscosity η_b. A Bingham plastic obeys the flow law

$$\sigma = S_y + \eta_b \dot{\varepsilon} \quad (1)$$

relating shear stress σ to shear strain rate $\dot{\varepsilon}$. More complex and general flow laws might be more accurate models of real materials, e.g., a pseudoplastic model with a power law relation between shear stress and strain rate. Although pseudoplastic models are most easily fit to experimental data, the Bingham model is often an adequate approximation, and it is the model of choice for many geological problems because it leads to complete and simple models of flow processes which demonstrate reasonable agreement with field observations [*Hulme,* 1974] and laboratory measurements of actual lavas [*Shaw,* 1969; *Moore,* 1987]. The Bingham model will be used throughout this paper; viscosity, denoted simply η, should be taken to mean Bingham viscosity, except where otherwise specified.

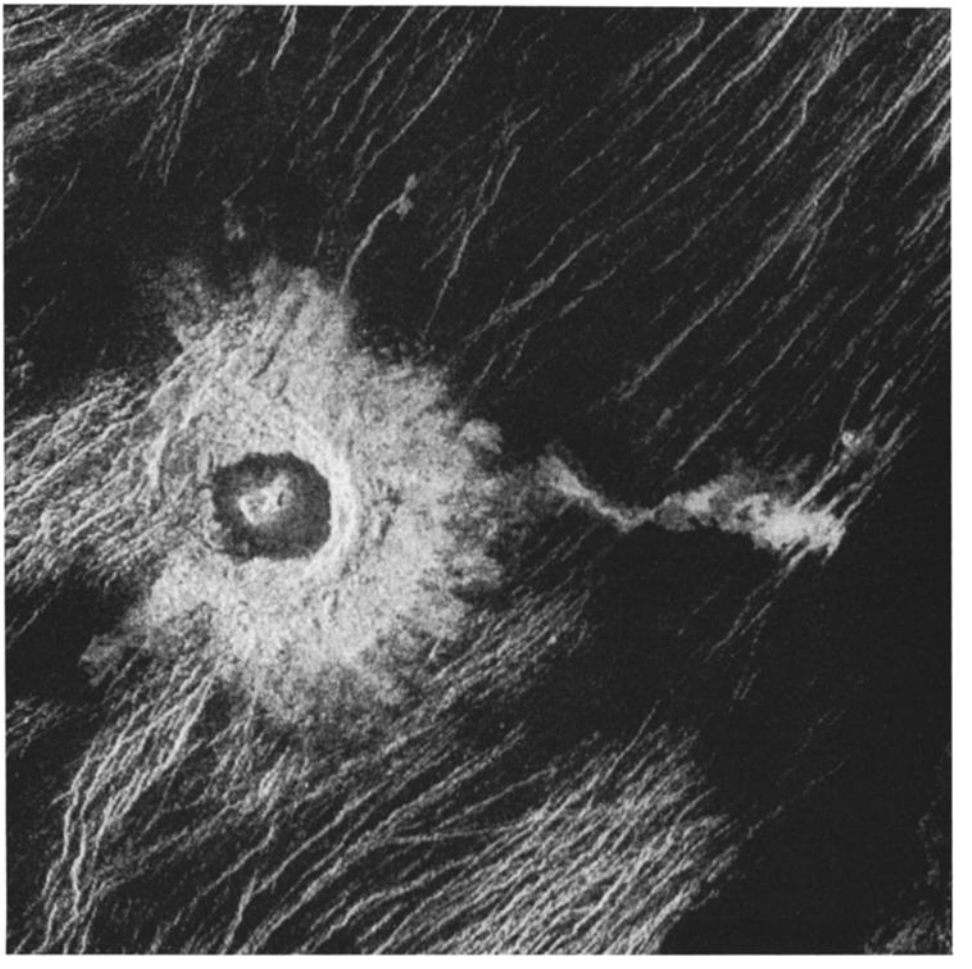

Fig 5. Kemble (47.7°N, 14.9°E; diameter 25 km). Magellan full-resolution radar image. Note simple bright flow to due east.

Hulme [1974] developed a complete model for the unconfined flow of a mass of ideal Bingham plastic fluid extruded from a small source onto a smooth inclined plane. This model serves to approximate the deposition of fissure-extruded material onto a sloping surface free of preexisting channels or complex topography given values of slope, density, gravity, effusion rate, viscosity, and yield strength. The Hulme model can be combined with morphological measurements of crater outflows to solve approximately the inverse problem of determining the yield strength and viscosity of the outflow material. Interest in the Bingham model for rheology is justified a priori by the observations that lava flows often stop on a slope on time scales shorter than cooling times (rather than ponding in depressions as Newtonian fluids would) and that lava flows cease to spread laterally absent topographic obstacles and before surface tension becomes significant.

Hulme's model assumes an isothermal flow with a dynamically unimportant solid crust, estimates of the growth times of solid crust show that the lateral spreading of a silicate melt flow is arrested before the crust is strong enough to contain it, and the melt should be approximately isothermal in cross section and over reasonable longitudinal distances if cooling is restricted to a thin crust. The approximations made are most valid for a flow much wider than it is high.

Lateral or downhill flow occurs only when the shear stress at the base of the flow exceeds the yield strength. Downhill basal shear stress at any point is proportional to the thickness of material ζ above that point, so there exists a critical depth ζ_s below which no flow occurs. Along either edge of the flow, there must be a region where $\zeta < \zeta_s$, since ζ approaches zero at the lateral boundaries. There will be no longitudinal flow in these regions; they will form stationary levees bounding the channel (i.e., the region where $\zeta > \zeta_s$; this is different from the usage of "channel" by *Baker et al.* [1991] and does not imply erosion). If w_b is the width of one stationary levee, *Hulme* [1974] derives the relation

$$w_b = \frac{S_y}{2g\rho\alpha^2} \tag{2}$$

where g is the acceleration due to gravity, ρ is density, and α is the slope of the underlying surface. Figure 14 shows a diagram of the ideal predicted flow profile and an illustration of the various width measurements used in the model.

Thus, given a measurement of the slope of the surface (assumed constant), the width of the flow, and the width of the levees or margins at a given profile across the flow, (together with the acceleration due to gravity and an assumed density), we can estimate the yield strength at that profile:

$$S_y = 2w_b g\rho\alpha^2 \tag{3}$$

as well as the central (and maximum) depth of flow at that point:

$$\zeta_0^2 = 2ww_b\,\alpha^2. \tag{4}$$

Integration of the profile function given above gives the cross-sectional area of the flow:

$$A = \frac{2}{3} w\,\zeta_0, \tag{5}$$

which will allow an estimate to be made of flow volume, given a

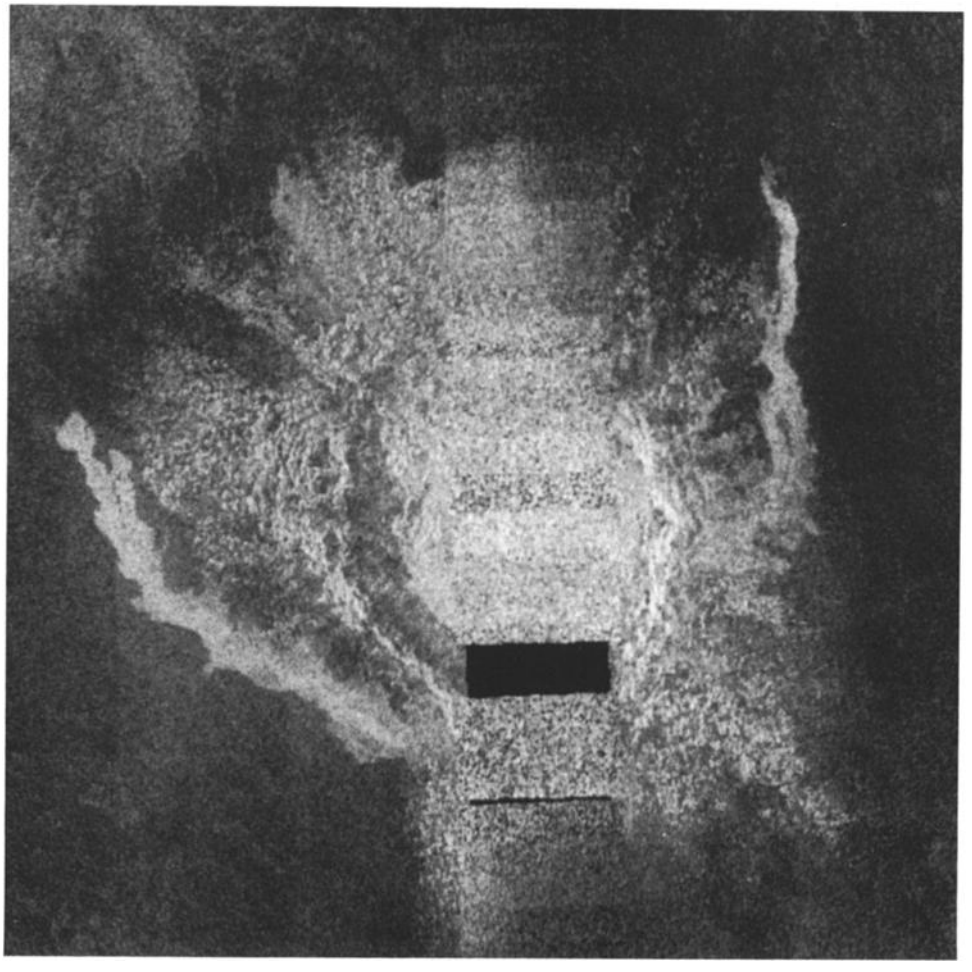

Fig 6. Parra (20.5°N, 78.1°E; diameter 48 km). Magellan full-resolution radar image. Poor data on orbit through center of crater resulted from tape recorder errors aboard the spacecraft. Regional gradient dips to northwest. Two bright flows originate on uphill side of crater, turn, and flow downhill to northwest.

measurement of flow length. Use of this model to analyze crater outflows introduces the additional assumption that the observed final deposit has the form of the critical profile, i.e., the deposit continues to reflect the form which the flow assumed at the time it ceased to move.

Other workers have derived different equations for estimating yield strength from remote observations of morphology: *Johnson* [1970] arrived at

$$S_y = \rho g \zeta_0 \sin\alpha, \tag{6}$$

whereas *Moore et al.* [1978] used

$$S_y = \frac{\rho g \zeta_0^2}{w}. \tag{7}$$

Moore et al. [1978] showed that the three methods (of *Hulme* [1974], *Johnson* [1970], and *Moore et al.* [1978], respectively) give results consistent to within a factor of 2, despite the large uncertainties involved in the Bingham model itself, unknown preflow topography, and the difficulties of remote measurement. The *Hulme* [1974] model is used here because there is no way to measure ζ_0 for low relief flows on Venus, and in Hulme's model, ζ_0 is a derived result rather than an input.

Real flows are likely to spill over their levees due to changes in the effusion rate over time. This process has been observed on active Hawaiian lava flows [*Fink and Zimbelman,* 1986]. The resulting spill-over deposits create an additional element of the flow structure, outboard of the levees, called margins. In remote measurements, it is often not possible to distinguish between flow levees and flow margins. Fink and Zimbelman detemined that where both are observed, it is an acceptable approximation to use combined margin and levee widths as input to Hulme's model.

Hulme [1974] also develops a method for estimating the product of volume flow rate and Bingham viscosity, $F\eta$, from the morphology of the flow. In order to obtain a viscosity estimate from this method, it is unfortunately necessary to guess the flow rate. Most work using this kind of model has chosen to adopt values of viscosity from known lavas with yield strengths similar to the calculated value and thereby derive an estimate of flow rate. For this study, in which the end goal is to obtain viscosity, such an approach is not helpful. Instead we choose to estimate the flow rate and derive a corresponding estimated viscosity. Flow rate is a very poorly constrained quantity, however, unless we introduce basic assumptions about the nature of the process. If we make the (perhaps unrealistic) assumption that the material is a steadily extruded melt which cools as it flows, then the work of *Head and Wilson* [1986] on cooling of lava under Venus conditions allows us to relate flow length and flow rate. Head and Wilson treat cooling by radiation and convection to the atmosphere, neglecting conduction to the surface. Their result is

$$F = \frac{180 \kappa w X}{\zeta_0} \tag{8}$$

where k is the thermal diffusivity (about 7×10^{-7} m^2 s^{-1} for most silicate melts) and X is total flow length. Obtaining F from (8) and $F\eta$ from Hulme's method, η follows immediately. Given our

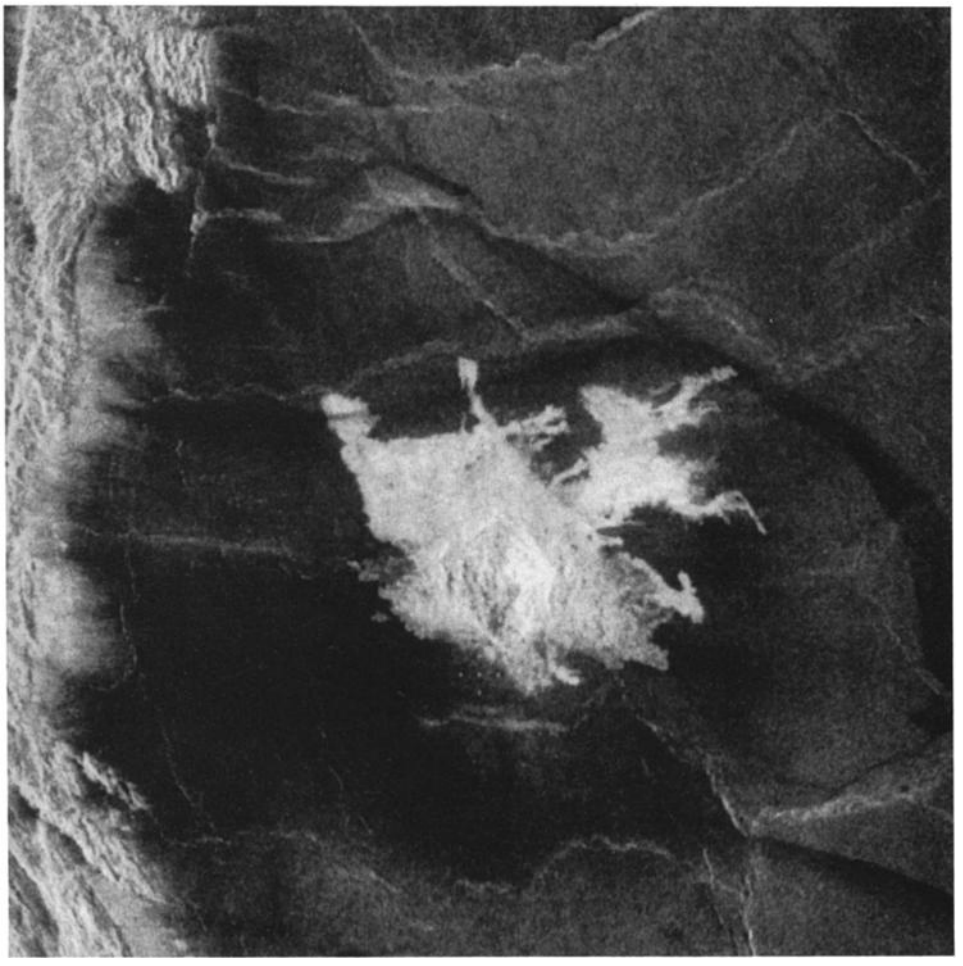

Figure 7. Small crater temporarily named Navka-7 (16.5°N,334.4°E; diameter 6 km). Magellan full-resolution radar image.

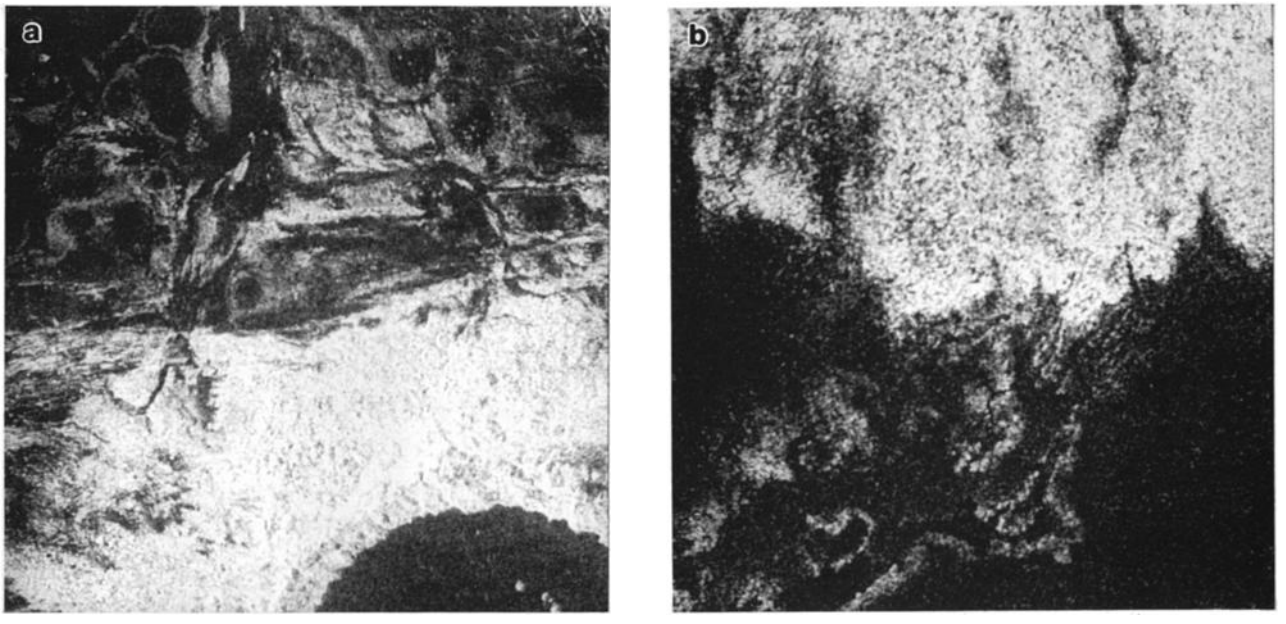

Figure 8. Stratigraphic relationships between ejecta and outflows. Magellan full-resolution radar images. (*a*) Aglaonice (Figure 1*a*) close-up, showing modification of ejecta blanket by outflow source area. Width of field 77 km. (*b*) Danilova (Figure 1*b*) close-up, showing no modification of ejecta edge of outflow. Width of field 38 km.

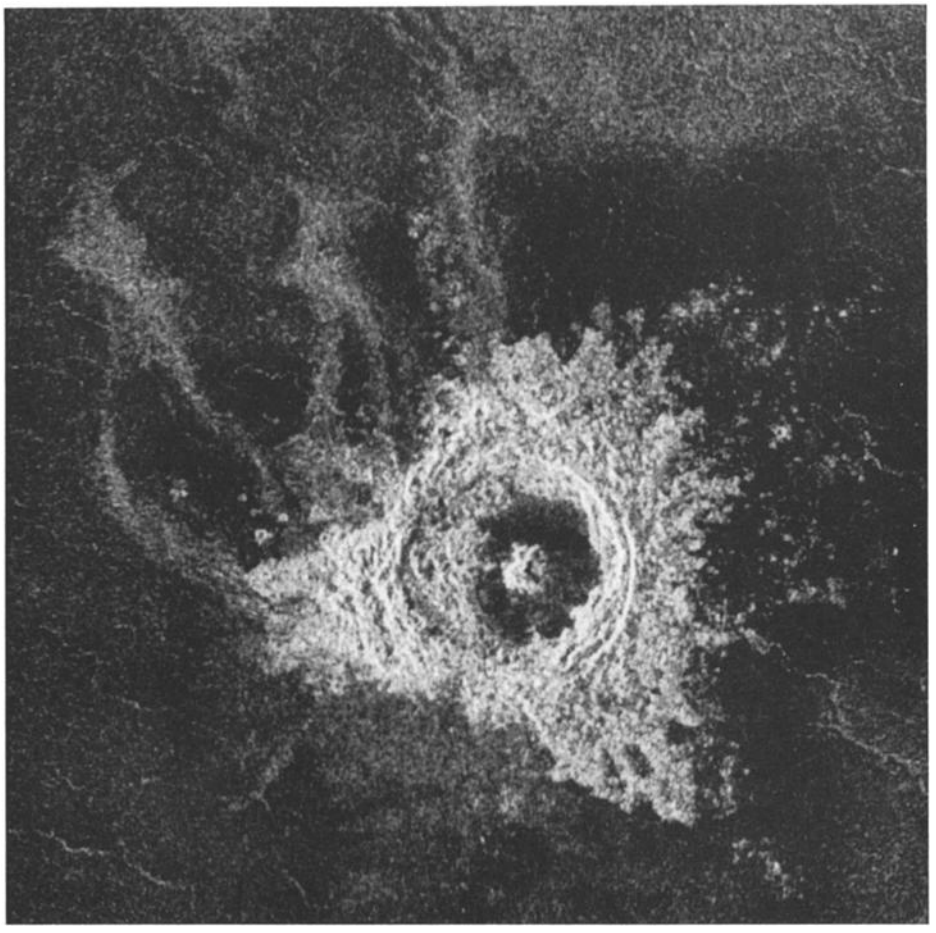

Figure 9. Crater Jeanne (40°N,331.4°E; diameter 20 km). A crater with a probable oblique impact direction to NNE but outflows which originate on the northwest and west sides of the crater.

intent to keep an open mind concerning the nature of the flowing material and its process of emplacement, however, the assumption that flow length is governed by melt cooling is very limiting. We will estimate η using Head and Wilson's method but restrict discussion of the resulting value to consideration of melt rock flow models. Although the value of viscosity may not be meaningful for debris flows, the effusion rate ought to be roughly constant along a flow (once the levees are established). Therefore the downstream trend in viscosity, whatever the absolute values, may represent a real trend for debris as well as for melts.

There are several problems to be considered with the use of this model for the problem at hand:

1. The Bingham plastic model may not meaningfully approximate the flowing material at the strain rates which it experienced in flow. This should not affect the calculation of yield strength, as Newtonian rheologies do not lead to levees or margins, and pseudoplastic models should approximately mimic Bingham behavior (levees are very slowly flowing in pseudoplastic models as opposed to truly stationary). It should be noted, as well, that most of the rheological parameters collected in this paper for comparison purposes were computed using Bingham models by other authors and that there is a general consensus in favor of the Bingham model as a useful approximation.

2. The models of *Hulme* [1974] for flow morphology and of *Head and Wilson* [1986] for cooling rates were developed assuming constant effusion over a span of time. If the crater flow deposits result from impact processes, however, then the material was certainly supplied in a single burst on an extremely short time scale. There is no simple way to correct for this difficulty, but it is possible that broad disorganized crater outflows such as that at crater Stuart (Figure 1*d*), which lack any channel-type morphology, may result from a sudden splay of fluid, while channelized outflows such as at Danilova (Figure 1*b*) may represent more protracted effusion. In any case, the model of *Hulme* [1974] should still give a valid approximation of yield strength, being essentially independent of flow rate. The calculated viscosities, however, are inversely related to the assumed effusion rate, so they may be erroneously high by many orders of magnitude if the flow material was supplied by a rapid process: apparent flow emplacement times (the ratio of estimated volume to assumed volumetric effusion rate) are of the order of days, whereas actual emplacement times may have been of the order of minutes.

3. There may have been large energy and pressure sources acting on the flows due to impact processes which might invalidate the simple model based on gravity alone [*Schultz*, 1991*a*]. The impact energy may be coupled to the flowing debris by means, e.g., of an elevated transient crater rim, in which case the slopes measured at the present era would not be meaningful. Additional energy sources are difficult to correct for in the case of melt-rock flows, but may in fact be necessary to explain the very

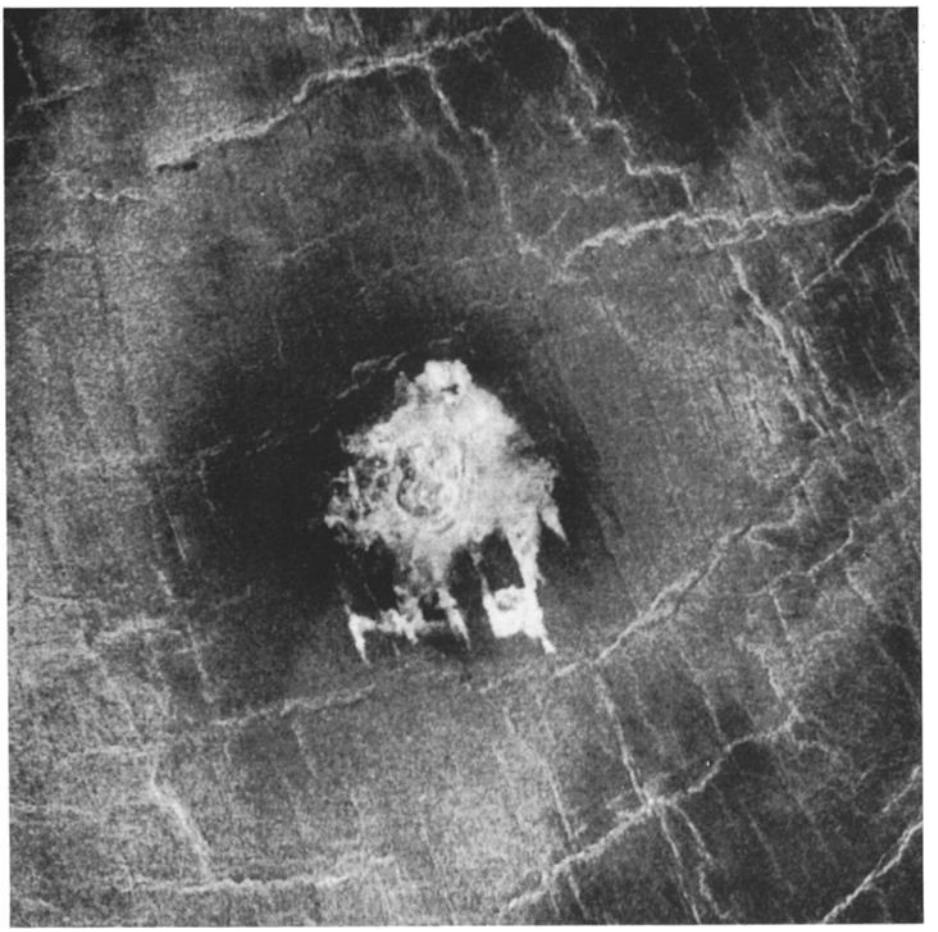

Figure 10. Structural control of outflows. Temporary name Fortuna 2 (34.6°N,5.5°E; diameter 6 km). Magellan full-resolution radar image. Note local fractures or faults in two directions which channel and contain outflow material.

low observed slopes in the case of debris flows (see below under Debris flow scenarios).

4. The identification of the observed deposits as channels and levees or margins may be incorrect. This is a matter of interpretation. For single flow events it is difficult to propose any other interpretation of the observed morphology, but the observed deposits could result from multiple flow events: a unit composed of several discrete flows would have a figure different from that predicted by Hulme's model. This would render the analysis irrelevant. Some of the deposits are exceedingly complex and likely result from multiple flow events. We have chosen for this study, however, only the simplest and most straightforward deposits or sections of deposits, those which appear to result from single events. Nevertheless, there may be spurious interpretations included in the data set. Furthermore, there is the potential for major bias due to selection effects. Many flows are excluded from the data set because no levees or margins can be detected. It is possible that their flow levees are too small to be resolved by Magellan imagery or that the radar viewing geometry is unfavorable or that there are no levees. There is no way to distinguish among these cases. Flows with Newtonian rheology, however, should they be present, would be systematically excluded, since they do not form levees or margins.

METHODOLOGY

The raw data for this study were synthetic aperture radar (SAR) mosaics and radar altimeter topography maps from the first cycle of orbital data taken by the Magellan mission. The full-resolution images have a pixel size of 75 m and are in sinusoidal projection. Altimetry has a pixel size of 4.641 km; this low resolution makes accurate slope determinations for small-scale local features difficult. Seventeen suitable flows were identified in the data available as of October 1, 1991 (covering roughly 80% of the Venus surface; see Table 1). Flows were included in this study only if a clear channel-and-margin morphology was evident and only if the slope could be measured. Many examples were excluded because their complex morphology made interpretation ambiguous. The flows are referred to hereafter by the name of the crater with which they are associated (some of these names are unofficial, pending approval by the International Astronomical Union nomenclature committee) plus a modifier such as flow direction if necessary. The widths of apparent levees or margins and of central flow channels were measured along regularly spaced lines perpendicular to the central axis of the flow; at least five lines were measured for each flow. The total length of the flow was estimated, and the slope of the flow was determined using the altimetric elevations of at least two points, near the origin and terminus of the flow respectively. The measured flow widths, margin widths, length, and slope were used to calculate yield strength, central depth, and product $F\eta$ at the location of each measured line across the flow. A locally calculated estimate of flow rate F is then used to approximate η at each location. These estimates of S_y, ζ_0, and η were combined to compute average values for each flow and were also retained individually for an analysis of the change in flow properties with distance along the flow. These calculated parameters allowed us to compute several additional properties of the flow, including flow volume, estimated mass, and apparent emplacement time scale.

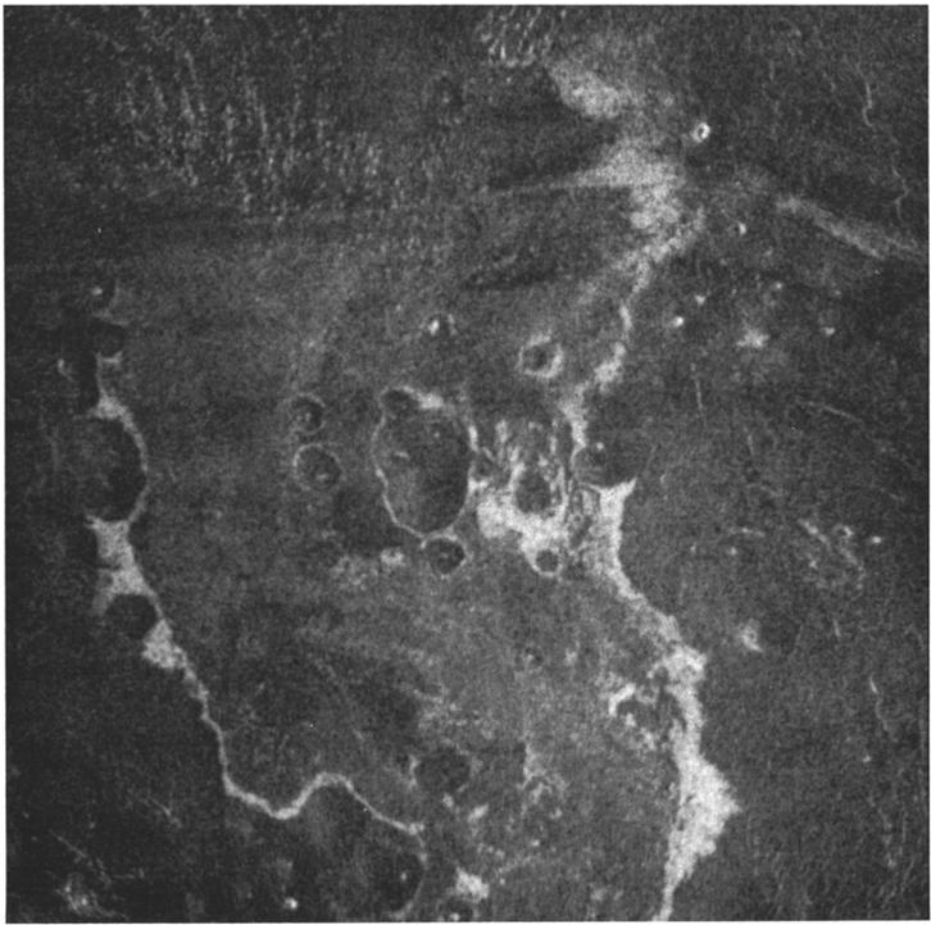

Figure 11. Small shields surrounded by Aglaonice outflow (Figure 1*a*), showing "bathtub rings" at high-water mark of outflow and summit pits, indicating volcanic nature. Magellan full-resolution radar images. Width of field 78 km. Note also apparent windstreaks and possible dune field in northwest corner of frame.

The width measurements are generally accurate to about 200 m where channel and levee or margin are explicitly identified; interpolation between unresolved levee segments may introduce errors of unknown magnitude. The length estimates should be accurate to within about 5 km. The reported elevation of each pixel in the topography data represents an estimate of the average elevation of a region 4.641 km on a side. The value is obtained by fitting templates to the altimetry radar echo and is subject to large errors if the topography of the target region is complex, i.e., if the actual elevations in the 21 km^2 represented by one pixel range far from the average value. An attempt was made for each crater outflow to identify artifacts and resolution effects in the altimetry data by visually inspecting topographic contour maps of the area; some limited qualitative corrections were made. Elevations have a nominal relative accuracy is 15 m; the absolute accuracy of the measurements is unimportant [*Pettengill et al.*, 1991]. The error in slope is largest for shorter flows.

The observed present-day slopes may differ from the slope at the time of impact due to later tectonic events or impact related vertical deformation. There is no way to correct for such changes in slope if they have occurred, but the extremely low values of the measured slopes are highly consistent among the 13 observed flows, in different tectonic regimes. If the slopes have been modified, a few anomalously low values might result from tectonic tilting, but a systematic effect such as differential uplift surrounding an impact event must be invoked to explain the consistency of the low slopes. This source of error could be tested through modelling of the uplift history associated with impact events.

The density of flow material is everywhere assumed to be 2500 kg m^{-3}. This value is appropriate for most melts but is undoubtedly high for many debris flow phenomena. The results generally scale linearly with density, however; consequently, the total range of reasonable densities introduces an uncertainty in yield strength estimates of perhaps a factor of 5. It should be kept in mind, then, that order of magnitude comparisons are the best that should be expected from this method.

This analysis was performed on the 17 selected crater outflow features as well as on two channelized Venus lava flows, one terrestrial mudflow deposit, and one terrestrial nuée ardente deposit. The results are presented in Table 3. The results for viscosity and yield strength are also shown graphically in Figures 15 and 16 along with viscosity and yield strength data from a variety of other flow processes, for purposes of comparison.

Scenarios and Controls

The intent of this section is to review the two classes of possible scenarios for the formation of fluidized crater outflows on Venus and to consider the range of predictions of each scenario. It is hoped that by collecting rheological analyses of various flows elsewhere in the solar system we may find an analogy which matches the results at hand. Many of the collected analyses serve the double purpose of control and analogy, where other authors have measured rheological properties by different methods (notably direct field measurement on Earth), if adequate maps and topography are available, we may apply our analysis and compute independent estimates of the measured properties.

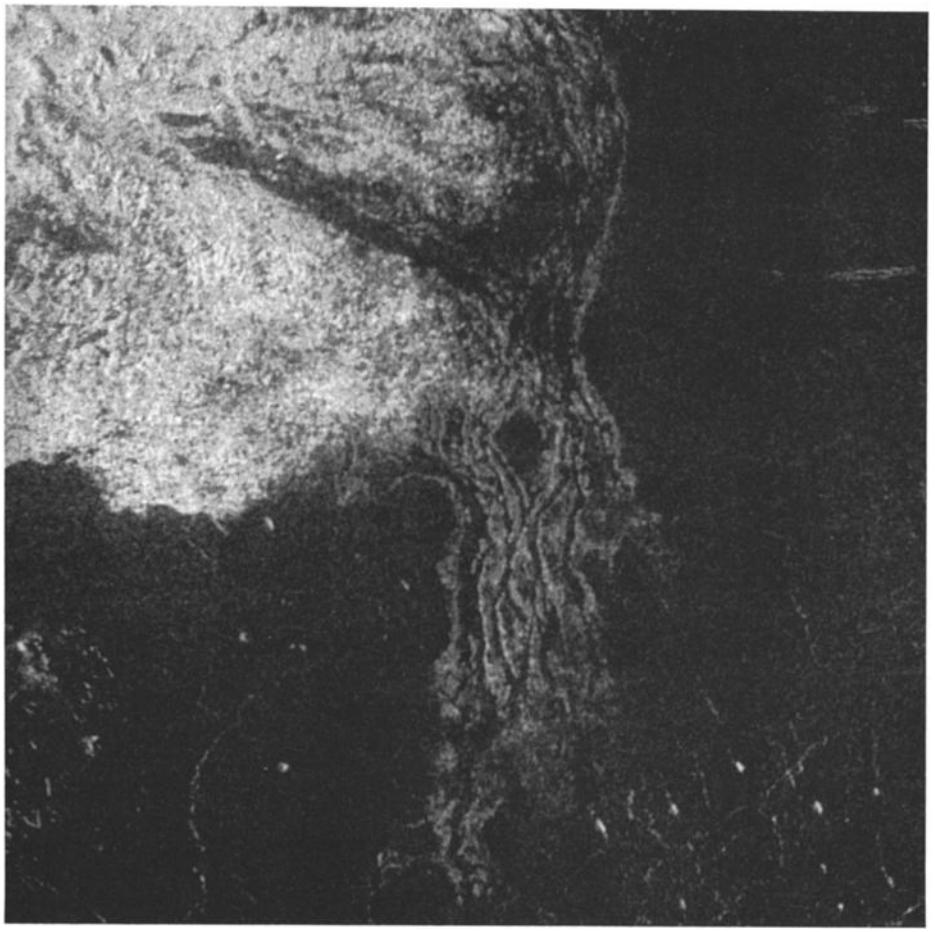

Figure 12. Southeast flow from Aglaonice (Figure 1*a*). Magellan full-resolution radar image. Note multiple channels with simple braiding morphology. Width of field 78 km.

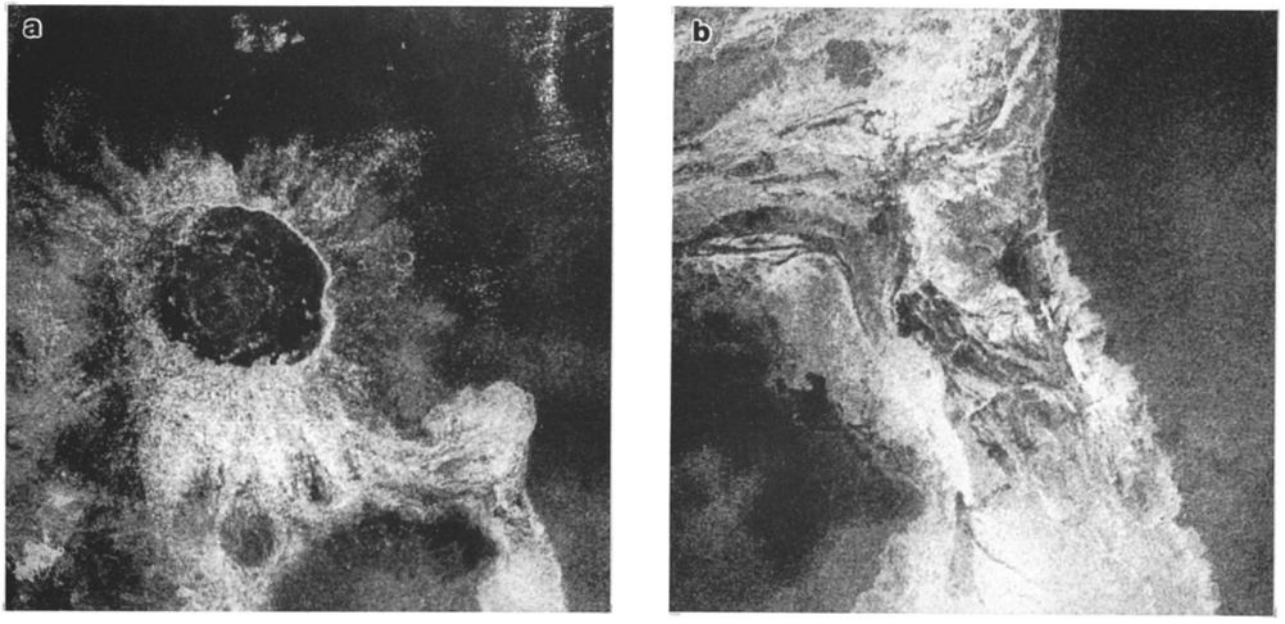

Figure 13. The second largest crater seen to date on Venus, Isabella (30°S,201°E; diameter 175 km). Magellan full-resolution radar images. (*a*) Overview, showing dark floor with concentric fractures and vague domical uplift but no central peak feature and large outflow compex to south and southeast. Note channel and drainage delta layout of large outflow to southeast. (*b*) Close-up of large outflow to southeast, showing complex, anastamosing multiple channel morphology and drain-out region. Width of field 115 km.

This technique may confirm the usefulness of our methodology. Furthermore, the available set of measured or estimated properties of different flow phenomena provides the basic framework for interpretation of our results. Estimates of yield strength and viscosity are meaningless in themselves, except when compared to the same properties as measured for known materials.

The Cratering Process

All the scenarios to be considered are intended as analogies for some process associated with impact cratering on Venus. Although much of the discussion will have little to do with impacts, the various candidate flow processes are only relevant insofar as something similar might be triggered by an impact. The possibility that the outflow features are not genetically derived from the impact is not considered. Ideally this study should reveal why the cratering process results in these outflows on Venus but not elsewhere (if they have been produced on Earth, it is possible that we would not have recognized them due to poor preservation of deposits). There are at least three stages in the cratering process which could provide source material to the flows, in vapor, melt, or solid form: (1) jetting, (2) vapor cloud expansion, and (3) ejecta emplacement.

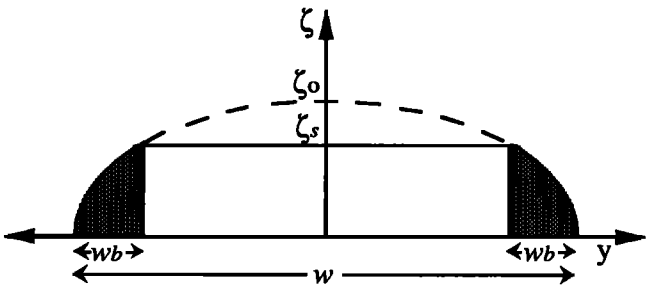

Figure 14. *Hulme* [1974] model for Bingham plastic flow on smooth inclined plane. Cross-sectional view of flow, showing stationary levees of width w_b along either edge. Total flow width is w, maximum potential depth at center line is ζ_o. Critical depth for initiation of flow is ζ_s.

1. Immediately on impact, particularly for more oblique impacts, there may be "jetting" of high-temperature molten and vaporized material in both the uprange and downrange directions due to development of regions of extraordinarily high pressure at the interface between impactor and target. This process is over quickly, by the time the impactor has penetrated half its diameter into the target, but on the order of one projectile mass of projectile plus target material may be ejected (reviewed by *Melosh* [1988]). The minimum mass of a projectile which can penetrate Venus's atmosphere without being decelerated too much to make a hypervelocity crater is of the order of 10^{12} kg, comparable to the estimated mass of the largest observed flows [*Phillips et al.*, 1991]. The form that a deposit of jetted material on Venus would take is not known; it depends on the interaction of jets with a dense atmosphere. This subject is not well studied, but it may be similar to Schultz's picture of vapor cloud interactions (see below).

2. The next relevant phenomenon is the expansion of a vapor cloud or fireball. The target and impactor material vaporized by the impact is produced at extremely high temperature and pressure, and it rapidly expands, overtaking early ejecta and forming a strong shock front (reviewed by *Melosh* [1988]). It may entrain some solid material, and it will begin to condense to liquid or solid particles as it expands and cools adiabatically. The character of the resulting expansion in understood in broad outline for near vertical impacts. On a planet with an atmosphere, the cloud expands until its pressure equilibrates with the atmosphere. The effects of oblique impacts are less well known. Some recent laboratory-scale experiments, however, have shown that in low-angle impacts the vapor cloud or fireball could be produced with substantial forward momentum, and it might be contained by the high atmospheric pressure on Venus and channelled into a ground-hugging turbidity flow or surge, rather than a classic hemispherical or mushroom cloud [*Schultz*, 1991*a*]. The mass of material vaporized should be at least several times the mass of the projectile, and thus the vapor cloud would contain easily enough mass to supply the observed flows.

TABLE 1. Basic Data for Sample of 14 Venus Impact Craters and 17 Associated Outflows

Crater Name	Location	Diameter, km	Apparent Impact Direction[a]	Flow Name[b]	Length, km	Slope, rad[d]	Azimuth of Origin
Aglaonice	-26.2, 339.7	63	V		180	0.001	N,SE[c]
Andami	-17.5, 26.5	28	?		30	0.006	W
Banzhao	17.2, 147.0	39	N		80	0.002	NNE
Danilova	-26.6, 337.2	48	SE		83	0.003	N,S[c]
Dickinson	74.6, 177.3	69	ENE		100	0.001	NNE
Edgeworth	32.2, 22.8	29	SW	south	20	0.003	SSE
				southwest	20	0.005	SW
Kemble	47.7, 14.9	25	NE		40	0.003	E
Lafayette	70.3, 107.5	39	S		65	0.005	S
Luce	-26.3, 31.3	38	SSW		30	0.003	S
Macdonald	30.0, 121.1	20	?		50	0.005	SW
Parra	20.2, 78.1	48	SE		60	0.008	SSW,E[c]
Potanina	31.6, 52.4	90	?	east	50	0.003	ENE
				northeast	50	0.002	NE
Voynich	35.4, 55.9	50	?		100	0.002	WSW
Xantippe	-10.9,11.7	40	?	northwest	40	0.001	NW
				southwest	50	0.0005	SW

[a] Determined by R. R. Herrick. ?, unclear or no data; V, vertical.

[b] If different from crater name, i.e., when more than one outflow is used from a given crater.

[c] There are two outflows from these craters, although only one was included in this study.

[d] Accuracy of slope depends on length of flow. Slopes of longest flows are accurate to about 20%, of shortest to about 100%.

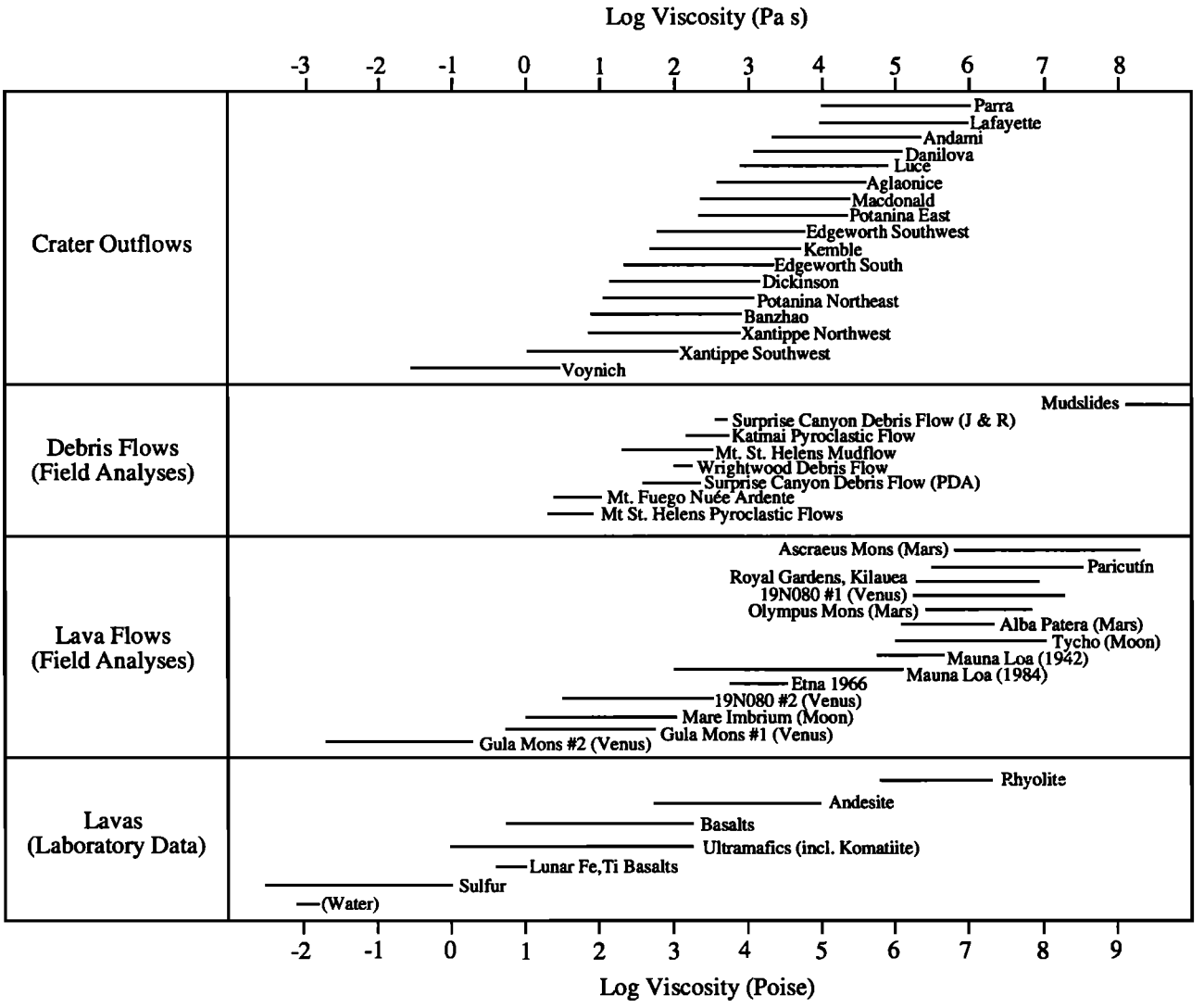

Figure 15. Results for viscosity analyses of 17 Venus crater outflows and reference viscosity measurements from field analyses of various debris flows and lava flows elsewhere in the solar system and laboratory analyses of magmas of several compositions. Citations for values from literature are in text. Lines represent estimated error ranges.

3. Finally, the ejecta proper, consisting of solid and molten target and impactor material, is subsequently deposited outside the crater rim. Ejecta masses are much larger than the estimated flow masses for the range of crater sizes observed on Venus. Ejection distances calculated for ballistic flight through Venus's atmosphere and gravity field show that the outflow features cannot result directly from simple ballistic emplacement. Nevertheless, ejecta blankets, in addition to jets and vapor clouds, are possible sources for fragmented, molten, or vaporized material outside the crater rims.

Melt Rock Flow Scenarios

The most basic division among emplacement scenarios is between melt and debris flows. Melt rock flows consist of rock or a mixture of rocks (normally silicate, but more exotic compositions have been considered) above the solidus temperature, with or without embedded crystals and a solid crust. The term "melt rock" is intended to include lava produced by partial melting in the Venus interior as well as impact melts, which may have unusual composition and may be at superliquidus temperatures. Debris flows consist of solid material, either alone or mixed with some mobilizing fluid (gas or liquid); fluid behavior of debris is an aggregate property. Hybrid models, e.g., debris flow with an interstitial liquid of silicate melt or melt rock flows with a substantial unmelted debris component, must also be considered.

If the observed outflow deposits result from melt rock flows, a mechanism is needed either to generate additional melt outside the crater or to remove melt from the interior of the crater and segregate it from other materials jetted or ejected. *Schultz* [1991*a*] favors supply of material by jets or vapor clouds. The temperature, pressure, and initial melt/vapor ratio of material comprising early jets is not well enough known to predict whether it will condense to a melt in a short enough distance to behave as a melt rock flow (but see *Schultz* [1992]). The condensation of classical vapor clouds is somewhat better studied, but it is not clear that a contained base-surge style vapor cloud should behave similarly or what fraction of it will condense to melt rather than to solid, and on what time scale. Thus the Schultz process could produce melt rock flows or debris-type flows and will be discussed in the next section as well. It is likely that melt condensed from a jet or fireball would be at superliquidus temperatures and in an extremely turbulent flow regime, such that

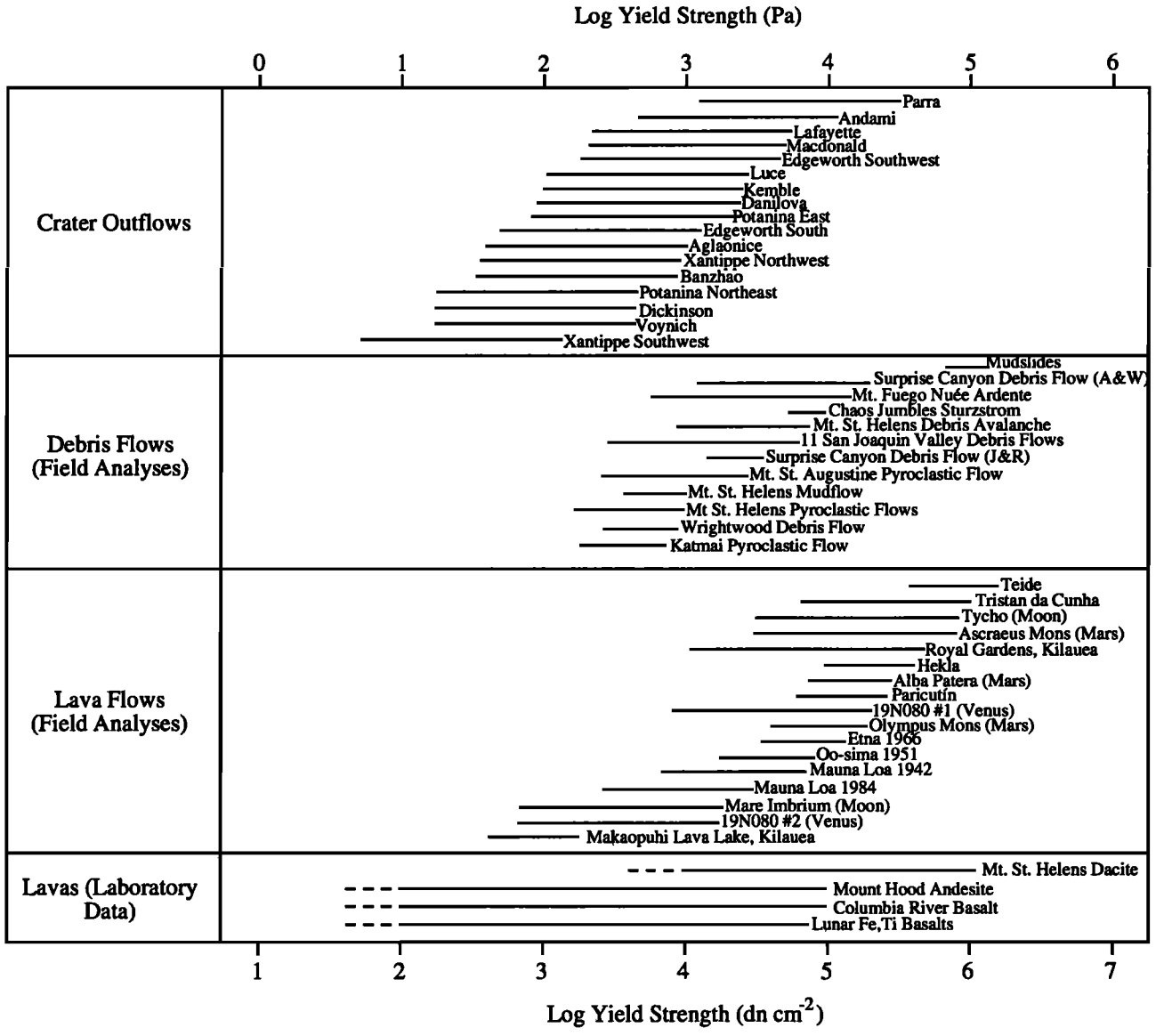

Figure 16. Results for yield strength analyses of 17 Venus crater outflows and reference viscosity measurements from field analyses of various debris flows and lava flows elsewhere in the solar system, and laboratory analyses of magmas of several compositions. Citations for values from literature are in text. Lines represent estimated error ranges.

its rheology may be quite different from that observed for normal lavas.

Baker et al. [1991] favor a source in the continuous ejecta and a mechanism wherein a melt fraction separates from and drains out of an ejecta blanket initially deposited as a mixture of melt and fragments. It is not known with any certainty how the melt and solid fractions of ejecta interact and whether the melt fraction can effectively separate from the solid fraction or what the rate of such separation might be. A mixture of melt and solid rocks is subject to several simultaneous processes, namely, cooling and crystallization of the melt fraction, heating and melting of the solid fraction, and separation of the fractions. Knowledge of the rates of these processes requires information about the compositions of the rocks, including volatile content, as well as the size distribution of solid fragments. The relationship between the flow source areas and the ejecta deposits ought to provide insight into this process, but the record is difficult to interpret.

Baker et al. [1991] use their model to explain the apparent modification of the ejecta blanket by flows such as Aglaonice (Figure 1*a*): there seem to be dark channels originating in the continuous ejecta and feeding into the outflow structure. Other deposits, however, such as nearby Danilova (Figure 1*b*), do not modify the ejecta blanket but seem to underlie and predate it. This stratigraphy, which is much more common, strongly implies that the outflow events generally precede emplacement of ejecta. This favors melt supply as part of the early processes (jetting and fireball), while airfall ejecta was still in flight.

Postimpact volcanism could occur through circumferential fissures beyond the rim, although no evidence for such fissures is seen. The frequency with which crater outflows occur, however, in a variety of tectonic settings, argues against this mechanism. In at least one case, the large crater Cleopatra, lava from the interior escaped through a gap in the crater wall; this mechanism is not evident at most other craters, which generally have remarkably intact rims and uniformly bright, unflooded inner terrace regions [*Basilevsky*, 1991]. Although postimpact volcanism can not be ruled out in particular cases, it is unlikely to be responsible for most of the observed outflows.

The various mechanisms for removing melt from the crater interior lead to definite predictions concerning melt properties and effusion process. The Baker model (draining of melt fraction from mixed melt-solid ejecta after emplacement) predicts slower effusion rates and cooler temperatures than the more violent Schultz model. The former mechanism ought to produce Bingham rheologies and leveed flows, whereas the latter scenarios (jet or vapor cloud supply) are likely to result in very hot, superliquidus melts with no crystal content, which would thus behave as Newtonian fluids with zero yield strength, unless other dispersed solids are incorporated to a significant extent (non-Newtonian properties of any fluid appear to arise from the presence of dispersed solids or crystals in suspension). This model this might be invoked to explain the majority of crater ouflows, which lack visible levee structures in Magellan imagery.

The most quantitative test available for distinguishing melt rock origins from debris origins and perhaps for distinguishing between melt rock supply scenarios, i.e., modelling of flow rheology, requires reference values of rheologic properties of lava and melt rock. The rheologic properties of melts are strongly dependent on composition and temperature, and are difficult to measure accurately even under ideal conditions. Values observed in the field vary widely among flows from various sources, among multiple flows from a given source and at different points along a given flow. Field values for viscosity and yield strength also tend to be as much as 2 orders of magnitude larger than laboratory values at the same composition and temperature. This implies the existence of time-dependent factors: continuing crystal growth at constant subliquidus temperature due to nonequilibrium kinetic constraints, as well as thixotropic properties such as progressive polymerization and ordering of undisturbed melt, will cause viscosity and yield strength to increase with time [e.g., *Fink and Zimbelman,* 1986]. For these reasons, it is generally more instructive to compare the properties inferred for crater outflows with field studies and with remote observation studies than with laboratory values. There is a universal tendency for both viscosity and yield strength to increase as lava cools and therefore to systematically increase in field observations along a given molten flow with increasing distance from the vent.

Both viscosity and yield strength increase strongly with silica content in silicate melts. Laboratory data from *Murase and McBirney* [1973] and other sources compiled by *Ryan and Blevins* [1987] are shown in Figure 15, along with computed viscosity estimates for the sample of 13 Venus crater flows analyzed. Errors for crater outflow viscosities are about ±1 order of magnitude. The results of this comparison will be considered below. Field measurements of various terrestrial lava flows are also summarized in Figure 15; these include values measured directly with a viscometer [e.g., *Shaw et al.,* 1968] and values inferred from Bingham flow models as described above [*Fink and Zimbelman*, 1986; *Moore*, 1987; *Hulme,* 1974 and references therein]. The general discrepancy between field and laboratory measurements should be noted.

Yield strengths for 10 terrestrial basalt flows are summarized in Figure 16. Field data on andesites, rhyolites, and other compositions are remarkably sparse, but laboratory data, showing viscosities 2-3 orders of magnitude higher than laboratory values for basalts, suggest that field measurements of silicic magma viscosities would probably be a few orders of magnitude higher than basaltic field values as well.

Comparison of flow viscosities. Using techniques similar to that of this study, several authors have analyzed various lava flows on other terrestrial planets (Mars, *Hulme* [1976], *Zimbelman* [1985] and *Cattermole* [1987]; Moon, *Hulme* [1974], *Schaber* [1973]). Results of a sample of these studies, including lunar flows and martian flows, are also shown in Figures 15 and 16. Included are the results of four analyses of Venus lava flows performed as part of this study. Two are from the south flank of the large volcanic edifice Gula Mons, at 19.6°N, 358.5°E and 19.5°N, 358.8°E, respectively. Two flows are from a corona-like feature at 19°N, 80 °E, originating at 18.1°N, 80.5°E and 19.5°N, 82.2°E. Being very small features, their slopes are somewhat uncertain, and thus the results are accurate to about a factor of 5 in yield strength and 2 orders of magnitude in viscosity. These flows, although small, were selected for their clear channel-and-levee morphology. No larger flows were observed with identifiable margins.

Baker et al. [1991] and *Kargel et al.* [1991] introduce the possibility of exotic melt compositions, including lunar Fe-Ti Mare basalts, komatiite, liquid sulfur, and carbonatite, to explain their observations on the Venus channels. These workers suggest that the same extremely low-viscosity (of the order of 10^{-3} to 10^{-1} Pa s) materials may also be responsible for the extended crater outflows, which they interpret as erosional channel features. There is no published discussion of any quantitative method used by Baker et al. or Kargel et al. to arrive at the viscosities of the crater "channels." Their qualitative analysis is explicitly dependent on the interpretation that crater outflows are erosional channels.

The relevance of terrestrial measurements as rheological analogues for Venus melts is subject to question. The variables affecting rheology of an effusive magma are composition, temperature, pressure, and effusion rate; the effect of the difference in each variable between Earth and Venus conditions needs to be examined. Venus surface compositions are very poorly constrained, having been measured (by gamma ray spectroscopy and X ray fluorescence experiments carried by short-lived landers) only a few times. Nevertheless, there is no reason to doubt that the compositions of most Venus basalts, which are thought to constitute the majority of surface rocks, fall within the broad range of compositions observed on Earth. The effects of the different temperatures at the surfaces of Earth and Venus are fairly easy to correct for, as viscosities are known over a range of temperatures. Much theoretical work has been done in this direction; *Head and Wilson* [1986] summarize the differences in cooling behavior that would be expected at Venus and Earth surface conditions. One variable that has not been sufficiently allowed for, however, is pressure. The surface pressure in the plains of Venus is about 90 atm. This prevents degassing of volatiles unless the initial concentration of volatiles in Venus magmas is exceptionally high (2-4 wt %). The consequences of this pressure effect on explosive volcanism have been considered at some length [*Wilson and Head*, 1983], but there may also be a strong effect on the rheology of effusive lavas. *Sparks and Pinkerton* [1978] showed that gas loss during fire fountaining in terrestrial basalts may be responsible for the non-Newtonian properties of basaltic magma. Specifically, gas loss causes large degrees of undercooling (i.e., it causes the temperature of the magma to decrease relative to the liquidus temperature) by (1) adiabatic decompression; (2) raising the liquidus temperature; and (3) forcing the magma to mix with cool atmospheric gases. This undercooling causes rapid crystal growth, which dramatically increases both yield strength and viscosity. As noted above, the presence of dispersed solids is the primary cause of non-Newtonian rheology in any liquid. Also, crystallization leaves an increasingly silica-rich liquid fraction with a higher viscosity.

Furthermore, this mechanism affects the entire flow, whereas simple cooling (by radiation, conduction, or convection) affects only the skin of a flow. Thus lava erupted at Venus pressures, unable to lose volatiles, will likely have highly retarded crystal growth and thus will maintain for some time a smaller viscosity and a much smaller yield strength than the same lava erupted at Earth conditions. We are presently unable to quantify this effect or evaluate its relevance for superliquidus melt rocks.

Debris Flow Scenarios

Most preliminary work on the Venus crater outflows has implicitly assumed a melt-rock flow origin (e.g., *Baker et al.* [1991], but see *Phillips et al.* [1991] for a more cautious viewpoint), but this assumption may be extremely limiting. The possibility of debris flow origins needs to be tested; it is possible that this will justify the focus on melts a posteriori. A wide variety of debris flow processes on several planets has been observed, many of which leave deposits superficially similar to the crater outflows on Venus. The term "debris flow" is used here in a very general sense, to describe a whole class of diverse processes, any fluidized transport or movement of fragmented solid rock, with or without interstitial fluid (e.g., atmospheric gases, vaporized rock, melted rock, or fines).

A debris flow with an interstitial fluid of molten rock is to be distinguished from a melt-rock flow by (1) the relative proportions of solid and melt, with solids being dominant in a debris flow, and (2) a solid component which did not crystallize from the melt fraction. In the classification scheme of *Pierson and Costa* [1987], nominally intended for differentiation among types of debris flows and debris avalanches, the most general term is "sediment-water flows", which is inapproriate for Venus, given the absence of water. The most relevant of Pierson and Costa's subclasses are "debris avalanche" and "sturzstrom", i.e., those flows sharing the following five characteristics: (1) a granular flow regime prevails (i.e., pore fluid pressure is less than hydrostatic pressure and the overburden is carried by grain-to-grain contact or collisions rather than buoyancy); (2) sediment concentrations approach 100%; (3) velocities are greater than 10 m s^{-1}; (4) the rheology is plastic; and (5) the interstitial fluid consists of air and/or fines and/or water. Pierson and Costa use "debris flow" in a much more restricted sense, to refer to a particular class of sediment-water flow with somewhat lower sediment concentration than debris avalanche, in which air is not an important intersitial fluid; this is not the usage intended here. Pierson and Costa's classification scheme was developed with only terrestrial flows in mind, and it needs to be generalized somewhat for our purposes. The (general) definition of debris flow adopted in this study is intended to embrace pyroclastic flows, including nuées ardentes, as well as rock avalanches.

The rheological parameters estimated for a number of debris flow phenomena are included in Figures 15 and 16 [*Beget and Limke*, 1988; *Eppler et al.*, 1987; *Limke and Beget*, 1986; *Fink et al.*, 1981; *Johnson and Rodine*, 1984; *Wilson and Head*, 1981; *Whipple and Zimbelman*, 1991]. Four major types of debris flow phenomena will be considered below: (1) debris flow in the strict sense, i.e., water mobilized, including mudflows [*Pierson and Costa*, 1987]; (2) pyroclastic-type flow, without any implication of volcanic origin [*Wilson and Head*, 1981]; (3) fluidized ejecta [*Schultz*, 1991*b*]; and (4) sturzstrom or debris avalanche [*Melosh*, 1979].

Water-mobilized debris flows. This category is included only because water-mobilized debris flows are common on Earth and have been the subject of several excellent rheological analyses; liquid water, of course, is not a candidate fluid on Venus. Field studies of debris flows (in Pierson and Costa's strict sense) in California using Bingham plastic rheology models have arrived at useful estimates of yield strength and viscosity. The observed yield strengths range from 100 to 6000 Pa, and apparent viscosities range from 50 to 1000 Pa s. It is not possible to convert these apparent viscosities to Bingham viscosities using the published data. It has also been observed that values of both parameters systematically decrease with distance along a flow, from source toward terminus [*Whipple and Zimbelman*, 1991]. This is attributed not to thixotropic properties of the material but simply to sorting processes wherein the lowest-viscosity fraction of material (generally, the finest particles) travels the farthest. As part of the present study, an analysis identical in procedure to that applied to Venus flows was applied to the large 1917 Surprise Canyon debris flow deposit in the Owens Valley. The analysis was done from maps drawn by *Johnson and Rodine* [1984], who also performed a rheological analysis of the deposit using somewhat different techniques (modelling the longitudinal figure of the toe and measuring runup at bends in the flow). Both analyses of the Surprise Canyon flow are presented in Figures 15 and 16. The results agree to much better than an order of magnitude. This was a water-mobilized debris flow; the relevance of the absolute values of these rheological parameters to Venus analogs is limited. The observed downstream trend, however, may be characteristic of debris flow processes in the general sense.

Pyroclastic like flows. Pyroclastic flows are extremely destructive, rapidly moving masses of hot volcanic gases and entrained fine solids, although they may also transport large blocks [*Wilson and Head*, 1981]. A subclass of pyroclastic flow is the nuée ardente, or glowing cloud, which generally consists of a dense basal flow and an overlying low-density cloud. Pyroclastic flows are similar in rheological character to water-mobilized debris flow, but they need not contain any water, and their density is much lower; they may be usefully described by a Bingham plastic rheology and may generate a recognizable channel-and-levee form deposit. Although pyroclastic flows are volcanic phenomena, the term "pyroclastic-type flow" might be loosely applied to a flow phenomenon regardless of its origin. A map of one nuée ardente deposit at Mount Fuego in Guatemala has been published by *Davies et al.* [1978], and this was analyzed as described earlier. Published results of some analyses of pyroclastic flows are also included in Figures 15 and 16 [*Beget and Limke*, 1988; *Limke and Beget*, 1986; *Wilson and Head*, 1981]. The process of emplacement of a pyroclastic flow is extremely attractive as a model for crater flows, from a strictly qualitative viewpoint: the jetting process or the vapor cloud/fireball associated with a large impact event on Venus, interacting with the atmosphere, might produce a ground-hugging turbidity surge, flow, or density current, which would probably resemble a pyroclastic flow in many ways. It would consist of a heterogenous ensemble of solid rock fragments, melt, rock vapor, and atmospheric gases with substantial forward momentum [*Schultz*, 1991*b*]. We might also consider that if the gas fraction of a pyroclastic-type flow consisted of vaporized rock as well as atmospheric volatiles, then the flow might convert downstream into a melt rock flow or a melt-mobilized debris flow, as the rock vapor condensed during flow. Although the mechanics and rheology of vapor cloud/solid mixtures in atmospheres are very poorly understood, it seems possible to first order that they might be analogous to pyroclastic flows produced by the collapse of volcanic eruption columns.

Pyroclastic-type flows could originate by containment of jetted material or vapor cloud material. The most useful distinction may be that for an oblique impact jets are directed both uprange and downrange, whereas the fireball flow travels only downrange [*Schultz*, 1991*a*; *Melosh*, 1988]. Some craters, naturally, have ejecta distributions suggesting near-vertical impacts; many of these also have outflows, e.g., Aglaonice (Figure 1*a*). Jetting may occur in such cases, but the direction would be arbitrary. Fireball containment as worked out above would not occur for vertical impacts. For oblique impacts (a more typical case than vertical), any deposit resulting from jet containment flow is likely to be seen in two opposite sectors, if it is present at all. In fact, some craters do have two flows, but they are not, in general, precisely opposite each other in point of origin. Also, two flows from different parts of a given crater are often very different in size and appearance, suggesting two different origins. Furthermore, most craters have flows originating in only one range of directions, which appears on the basis of ejecta patterns to be within 45° of the downrange direction. Also, the fireball involves a much greater mass of material than the jets, and fireball deposits would likely obliterate any earlier jet deposits. For these reasons, fireball containment flow appears to be the better candidate for origin of outflows from oblique impacts. Neither jet containment nor fireball containment is a likely process for outflows from near-vertical impacts.

Fluidized ejecta emplacement. Ejecta fluidization is observed in several diverse settings. Impact craters on Mars often have an ejecta morphology suggesting emplacement by flow (Figure 2*d*). There are flow features suggesting sedimentary bedforms (dunes, hummocks, radial ridges, etc.) in the ejecta of most impact craters on any planet, suggesting at least some flow after impact, perhaps simply as a result of the forward momentum of ejecta fragments when they land (ballistic sedimentation; see *Melosh* [1988] for review). The fluid character of Martian rampart craters is much more dramatic. Many theories consider the role of water from melted ground ice in the fluidization of Martian crater ejecta, but *Schultz* [1991*b*] has shown that fine material from the Martian regolith may act as a fluid in the absence of water. The fine-grained ejecta interact with the atmosphere to create a dry debris flow. This type of ejecta flow, if present, would follow and superpose any fireball vapor-and-debris flow (see above) that may have occurred. Fluidized ejecta flow tends to produce a rampart or low ridge at the terminus of the flows; no such ramparts are observed, but this does not rule out their presence. The Magellan radar is more sensitive to roughness than to topographic relief, so low ramparts might not be resolved.

Debris avalanches. Extremely large volume avalanches with anomalously long runout distances have been observed on Earth, as well as in the Valles Marineris on Mars and adjacent to crater Tsiolkovsky on the far side of the Moon (Figure 2*c*). *Hsü* [1975] and *Melosh* [1987] defined long-runout rock avalanches with a volume greater than 10^6 m^3 as sturzstroms, to be distinguished from large landslides (which move by sliding, i.e., deformation is concentrated at the base of the moving mass) by the fluid character of their motion (sturzstroms move by flowing, i.e., shear deformation pervades the moving mass). Hsü, noting that examples have been seen on the Moon, rejected models based on water or mud fluidization and models of sliding on trapped air cushions in favor of a model based on *Bagnold* 's [1954] concept of dispersive flow of cohesionless grains, in which an interstitial mass of fine rock debris supports the coarse fraction by direct grain-to-grain collisions.

Melosh [1979], rejecting the ability of grain flow to generate the observed runout distances, proposed a new process: the exceptionally high mobility of these flows in the absence of water or air results from "acoustic fluidization" (see also *Schultz and Gault*, [1975]). This is a speculative and controversial idea: confirmation or acceptance of it awaits more research, but it merits discussion here as a possible mechanism. Acoustic fluidization occurs when elastic pressure waves propagated through the solid phase by direct grain-to-grain contact randomly relieve the overburden pressure between adjacent grains and allow them to move [*Melosh*, 1979]. Acoustic fluidization should operate in a vacuum as well as in an atmosphere. The most appealing feature of these massive avalanche phenomena as an analogue for crater flows is their exceptional ability to retain kinetic energy over large distances; after gaining speed and energy by flowing down a steep gradient, they may continue across a flat region for several tens of kilometers and even climb over obstacles on the order of a hundred meters high.

It is observed that the "friction coefficient" *H/L* (i.e., the ratio of elevation drop to horizontal runout distance) shows a rough inverse correlation with flow volume. *Melosh* [1987] explains this correlation as resulting from the scale-dependent ability of a flow to retain acoustic energy, which is dispersed only from the surface of the flow and is therefore retained more efficiently in larger flows. As this energy is gradually lost during flow, the avalanche slows and eventually stops. This ought to result in a lava like increase in rheological parameters downstream. In order to test the correlation of *H/L* and volume for Venus crater outflows, it should be noted that the parameter *H/L* is related to the average slope down which the flow travels. Slope and volume are both determined in this study; the sample of crater outflows whose entire volumes were measured are plotted along with a number of large debris avalanches in Figure 17. The slopes under Venus crater outflows are exceptionally low, clearly different from the trend for ordinary large debris avalanches elsewhere; this implies that energy due to acoustic fluidization would probably be insufficient to transport the flow over the observed distances. The other avalanches plotted, however, obtained their energy only from gravitational potential, proportional to the vertical fall distance *H*. In the case of Venus crater outflows, we expect an additional large nongravitational energy source from the impact process, which would be transferred to the flow either by atmospheric shock wave or seismic wave. Consequently, large volume crater flows may be expected to have anomalously small friction coefficients. If the energy supplied by the impact shock replaces the early steep fall associated with most large avalanches, then the long runout distances can be explained in spite of the extremely low slopes observed.

We can estimate the magnitude of the energy which the impact shock would have to supply to the flow to provide the necessary impulse for acoustic fluidization (neglecting dissipation due to atmosphere). Such a calculation may be used to test the feasibility of impact shock mobilization of sturzstroms with the observed volumes and friction coefficients. This analysis was applied only to those six craters where the entire outflow deposit was measured, as opposed to the segments or subunits measured for the other 11 outflows. Using the average regression line shown in Figure 17, the difference between the *H/L* expected for the measured flow volume and the observed slope was obtained for each outflow. This was multiplied by the total length of the flows, leading to ΔH, the apparent missing fall height for the crater outflow. ΔH was multiplied by the acceleration of gravity to

obtain , $\Delta\bar{E}$ the specific energy or energy per unit mass apparently supplied to the flows to replace the missing gravitational potential energy as a source for acoustic vibrations. $\Delta\bar{E}$ can be compared with the melting and vaporization energies to investigate whether it is feasible to accelerate solid flows by this means. Finally, given estimated flow volumes and an assumed density, $\Delta\bar{E}$ was converted to an estimate of ΔE, the total nongravitational energy required. Table 2 compares this energy with order-of-magnitude estimates of the total energy of each impact. These impact energies are obtained from a scaling law (crater diameter α $E^{(0.3\pm.05)}$), calibrated from craters generated by shallowly buried nuclear explosions of known yield (reviewed by *Melosh* [1988] and *Glasstone and Dolan* [1977]). Table 2 shows $\Delta\bar{E}$, ΔE, the estimated impact energy, and the ratio of ΔE to estimated impact energy for the four crater outflows considered. The specific energies are substantially smaller than the heat needed to remelt igneous rocks, about 8 x 10^5 J/kg for a basalt initially at 730°K [*Basaltic Volcanism Study Project*, 1981]. Also, the estimated impact energies are 10^4 to 10^6 times greater than the desired nongravitational flow energies. It thus ought to be energetically possible to account for the difference between the typical slopes of sturzstrom deposits and the crater flows using an impact energy source.

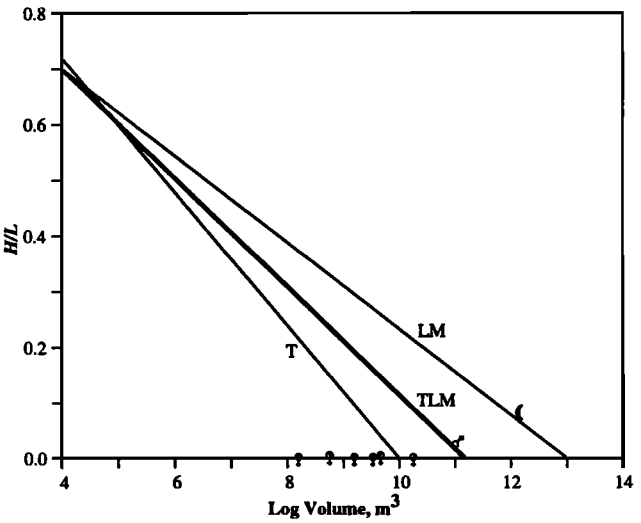

♂ Valles Marineris, Mars (Fig. 2*b*)
☾ Tsiolkovsky, Lunar (Fig. 2*c*)
♀ Venus Crater Outflows (Figs. 1*a*, 1*b*, 6, and 7, Table 2)

LM Lunar and Martian best fit, P. Shaller (1991)
T Terrestrial best fit, P. Shaller (1991)
TLM Terrestrial, Lunar, and Martian best fit, *Melosh* [1987]

Figure 17. Coefficient of friction *H/L* versus volume for large debris avalanches on Earth, Moon, and Mars, and for six crater outflows on Venus (those listed in Table 2). Light regression lines are from Shaller (personal communication, 1991), bold line is from data collected by *Melosh* [1987].

RESULTS

The average results of the rheological analysis for 17 Venus crater flows are shown in Table 3. The extreme range of the computed values of viscosity and yield strength reflects either a significant diversity of processes and materials or extremely large errors (or both). The average viscosity estimates are compared with the various reference viscosities in Figure 15. It is clear that the Venus crater outflow results as well as all the reference values cover many orders of magnitude in viscosity. Nevertheless, it is possible to draw some conclusions from the analysis. Most of the average viscosities of crater flows cluster between 10^2 and 10^4 Pa s. The observed viscosities are generally low compared to field observations of most terrestrial and Martian lavas. Some basalts, notably the 1984 flows from Mauna Loa and the 1966 flows from Mount Etna, match many of the calculated crater flow viscosities. There are a few flows with low viscosities in the range of lunar basalts, but there are none requiring nonsilicate exotic composition, except the smallest and therefore most uncertain flow at crater Voynich. Laboratory measurements of viscosity on lavas of different compositions, each of which is shown in Figure 15 for the entire range of temperatures between its solidus and liquidus, should be used with great caution, but they imply that the Venus crater outflows have a wide range of silica contents or temperatures. These results do not conclusiviely indicate composition, but if we weight field data more heavily than laboratory data, we may say that a melt rock flow interpretation favors a basaltic composition, at normal subliquidus temperatures. No conclusion should be drawn from viscosity values with respect to debris flows, since the method of calculation assumed lava flow cooling behavior.

The average yield strength estimates for Venus crater outflows are compared with the various reference yield strengths in Figure 16. These results are subject to much scatter and ambiguity, but the following observations seem reasonable. Most of the crater flow yield strengths fall between 10^2 and 10^3 Pa. The typical yield strengths of debris flows tend to be higher than these, but there is much overlap. In particular, yield strengths of pyroclastic flows are consistent with those of all but two or three of the crater outflows. The one yield strength estimate available for a sturzstrom is from Chaos Jumbles [*Eppler et al.*, 1987], 6000 to 10,000 Pa, which is higher than nearly all of the crater outflow values. This does not rule out avalanche type origin for the outflows, as fluidizing mechanisms in addition to acoustic fluidization or whatever mobilizes dry avalanches may have been active. A prominent example of such high fluidity, cited by *Hsü* [1975], is the Huascaran sturzstrom in Peru, which was exceptionally mobile due to an interstitial fluid of wet mud. This may be analogous to an avalanche from a Venus crater containing

TABLE 2. Comparison of Estimated Flow Energy and Scaled Impact Energy for Six Venus Crater Outflows.

Crater Name	$\Delta\bar{E}$, J/kg	ΔE, J	Impact Yield, J	ΔE /Yield
Aglaonice	2×10^5	10^{19}	10^{23}	10^{-4}
Banzhao	7×10^4	8×10^{16}	2×10^{22}	4×10^{-6}
Danilova	10^5	10^{18}	4×10^{22}	4×10^{-5}
Dickinson	2×10^5	6×10^{17}	10^{23}	5×10^{-6}
Kemble	10^5	10^{17}	2×10^{21}	5×10^{-5}
Parra	9×10^4	10^{18}	3×10^{22}	4×10^{-5}

Variables explained in text.

TABLE 3. Results of Bingham Plastic Fow Modelling for 17 Venus Crater Outflows, Two Venus Lava Flows, One Terrestrial Nuée Ardente and One Terrestrial Debris Flow

Flow	Mean Width, km	Mean Levee Width, km	Mean Central Depth, m	Mean Yield Strength, Pa	Mean Viscosity, Pa s	Total Volume, km^3
			17 Crater Outflows			
Aglaonice *	27.3	2.6	16	220	3600	24
Andami	4.3	1.3	13	1200	2200	1.0
Banzhao *	4.5	1.3	6.2	200	73	0.45
Danilova *	13.6	1.5	16	440	11000	4.5
Dickinson *	10.8	1.4	6.1	78	120	1.6
Edgeworth South	2.9	0.9	5.7	250	200	0.17
Edgeworth Southwest	2.5	0.9	10	900	550	0.28
Kemble *	3.4	1.1	8.2	450	400	0.39
Lafayette	8.5	1.2	21	1200	97000	4.3
Luce	7.1	1.2	12	470	7200	1.1
Macdonald	3.1	0.9	13	1200	2200	0.95
Parra *	5.7	1.9	39	6100	100000	4.9
Potanina East	6.5	1.1	10	380	2000	0.51
Potanina Northeast	5.5	0.7	4.5	83	95	0.34
Voynich	1.1	0.4	2.0	77	0.28	0.0095
Xantippe Northwest	7.8	2.6	8.6	210	70	0.62
Xantippe Southwest	15.6	2.3	4.1	24	11	0.86
			Two Venus Lava Flows			
19N080 flow 1	1.9	0.7	18	3600	7000	0.36
19N080 flow 2	8.6	3.2	12	380	140	1.9
			Two Earth Debris Flows			
Fuego nuée ardente *	0.029	0.0067	2.1	3000	5.3	-
Surprise Canyon *	0.050	0.0180	3.8	6800	86	-

* Complete outflow. All others are segments of flow with measurable levees.

rock vapor or melt. The yield strengths are also somewhat lower than typical values for observed lava flows, particularly silicic and Martian flows. There is reasonable agreement between the calculated yield strengths and those of 1984 Mauna Loa basalts (300-3000 Pa) and Mare Imbrium flows (near 400 Pa). Laboratory data on yield strength vary over a wide range as a function of temperature; near or above the liquidus yield strength is essentially zero, and near or below the solidus the yield strengths may be of the order of several megapascals. Thus the laboratory results are of little use because we can match a calculated yield strength to nearly any rock type by choosing an appropriate temperature. Data quoted in *McBirney and Murase* [1984] imply temperatures around 1175°C to match the yield strength for basalts and andesites, or around 1050 °C to match Mt. St. Helens dacite. Tentative conclusions from yield strength data, relying on field analyses, are (1) sturzstrom and pyroclastic-type processes are not excluded for most flows, although an additional fluidization agent may be required, and (2) a melt rock origin indicates properties broadly similar to basalt.

The apparent changes in viscosity and yield strength along Venus crater outflows from source to terminus may be important in differentiating between melt and debris flow processes. Assuming constant effusion rate along the flow, these trends are meaningful whether the actual effusion rate is known or not. There is considerable noise in all of the profiles, but Table 4 summarizes the trends apparent for all 17 outflows. An up arrow represents overall increase in viscosity or yield strength downstream, a down arrow represents an overall decrease, and a dash indicates a mixed, flat, or unclear trend.

Recall that melt and acoustically fluidized debris are expected to show increases in both viscosity and yield strength downstream and that debris mobilized by an interstitial fluid may show decreases in both parameters. For each crater outflow, upward trends in both viscosity and yield strength are taken to indicate "lavalike behavior" and downward trends in both parameters define "debrislike behavior." Among the 17 Venus flows, there are 10 fairly unambiguous debris flowlike trends, one unidentifiable trend, and six lavalike trends. None of the upward trends is as strong as would be expected for melt, e.g., at Mauna Loa in 1984, where Bingham viscosity increased 3 orders of magnitude from vent to toe. There is the possibility of significant error in the use of trends, since assumptions like constant slope and density may not represent the actual situation. Thus an outflow which travelled down a concave (steadily decreasing) slope would show an erroneous upward trend in yield strengths computed on the basis of constant slope. This type of error could be corrected by using a variable slope if higher-resolution topography data were available. The observation on downstream trends lead to two conclusions: (1) debris flowlike behavior is confirmed for most of the outflows, although (2) melt rock origin is implied for six of the 17 outflows.

Some insights may be gained by searching for correlations among various measured and/or calculated variables. Both *Hulme* [1974] and *Head and Wilson* [1986] published plots of viscosity versus yield strength for Bingham plastic models of silicate lavas. The Hulme relation is for average properties of flows of different silica contents, whereas the Head and Wilson curve is for a given material, anhydrous tholeiite basalt, at various temperatures. The 17 crater flows, separated into lavalike and debrislike flows, are shown in viscosity versus yield strength space along with the Hulme line in Figure 18. It is seen that eight of the flows plot on or near the Hulme line, one plots well below it, and eight plot well above it and that all 17 points clearly define a trend parallel to the Hulme line. The parallel trend may be a result of the fact that the same model was used by Hulme and by this study, in which viscosity and yield strength are not fully independent parameters.

It should be noted (Table 4) that of the six Venus flows with lavalike downstream trends, four plot on Hulme's line for silicate melts, whereas of the 10 outflows with debrislike downstream trends, seven plot well away from Hulme's line. Keeping in mind that the viscosity estimates are not meaningful for debris flows, it is reasonable to suppose that plotting well off Hulme's line is indicative of a nonmelt origin or an exotic melt composition.

Both viscosity and yield strength show direct correlations with the measured slope. This is true for the data in this study as well as the results of many analyses by other authors on a variety of natural flows [e.g., *Johnson and Rodine,* 1984]. This result is somewhat unsettling at first. The properties of a material ought to be independent of the slope down which the material flows. This correlation thus seems to imply a serious failure of the model used to obtain the material properties. This objection is probably valid for melt rock flows: the rheologic properties of melts are essentially intrinsic material properties, dependent on temperature, composition, pressure, and time. Debris flows, by contrast, have no intrinsic material rheology; their behavior develops only during flow and may reasonably be a function of the slope or other elements of the flow environment. In other words, an avalanche may flow down a 30° slope by a different mechanism and with a different apparent rheology than an avalanche of the same material and size on a 10° slope. The existence of this correlation may thus be construed either as evidence of a major flaw in the model or of debris flow origins for most of the modelled deposits.

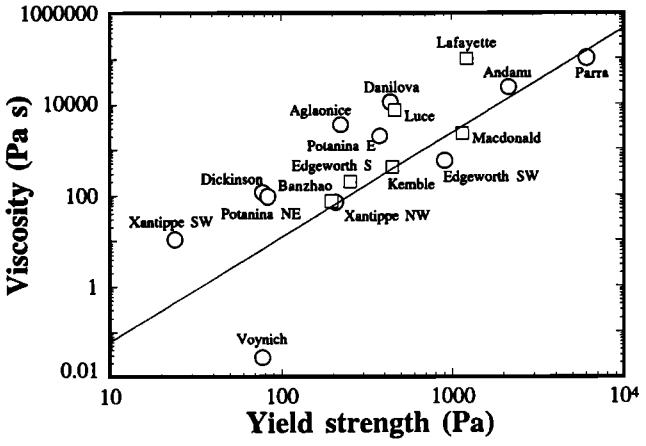

Figure 18. Viscosity versus yield strength for 17 Venus crater outflows. Circles are debris-like flows, squares are lavalike flows (see Table 4). Line shows estimated locus of values for silicate melts of varying silica contant [*Hulme* , 1974].

There is a set of additional qualitative tests that should be applied to any model for crater flow formation. A leading observation to be explained is the azimuth of the flows, with respect to the impact direction for apparently oblique impacts and with respect to local topography, as well as the narrowly focused appearance of some flows and the broad splay of other flows. Although at first glance the fireball containment model seems to imply a narrow flow oriented directly downrange, P. H. Schultz (personal communication, 1991) believes that the initial momentum from the impact is likely to transport the flow only one or two crater radii straight downrange from the point of impact, to a point which will eventually be beneath the ejecta blanket. Beyond this, the cloud may separate into vapor and melt phases, and the direction of subsequent flow of the vapor phase will be controlled by local topography [*Schultz,* 1992]. This is consistent with the "tangential" appearance of flows at crater Carson (Figure 1*c*) and the uphill point of origin coupled with subsequent downhill flow apparent on two outflows at crater Parra (Figure 6) on the flank of a topographic high associated with a nearby volcano. The fresh appearance of the crater implies that it probably postdates the volcano and the topographic high and so impacted upon approximately the present topography; there is evidence of extensive lava effusion from the volcano, but it does not bury or embay the crater. The appearance of the flows from Parra is strongly inconsistent, on the other hand, with the model of *Baker et al.* [1991] in which melt simply drains from ejecta after emplacement. This model would predict drainage on the downslope side of the crater, unless the topographic slope was reversed when the crater formed, in which case the U-turns seen in Figure 6 are difficult to explain. By contrast, the flows from Aglaonice (Figure 8), with broad source regions at the foot of the continuous ejecta blanket are more consistent with Baker's model.

TABLE 4. Downstream Longitudinal Trends in Viscosity and Yield Strength and Position With Respect to *Hulme*'s [1974] Relation Between Viscosity and Yield Strength for Silicate Magmas for 17 Venus Crater Outflows

Name of Flow	Downstream Trends			Position Relative to
	Viscosity	Yield Strength	Conclusion	Hulme's Trend
Aglaonice	–	↓	debris	above trend
Andami	↑	↓	?	on trend
Banzhao	↑	–	lava	on trend
Danilova	↓	↓	debris	above trend
Dickinson	↓	↓	debris	above trend
Edgeworth South	↑	↑	lava	on trend
Edgeworth Southwest	–	↓	debris	near trend
Kemble	–	↑	lava	on trend
Lafayette	–	↑	lava	above trend
Luce	↑	↑	lava	above trend
Macdonald	↑	–	lava	on trend
Parra	↓	↓	debris	on trend
Potanina East	↓	–	debris	above trend
Potanina Northeast	↓	↓	debris	above trend
Voynich	↓	↓	debris	below trend
Xantippe Northwest	↓	↓	debris	on trend
Xantippe Southwest	↓	↓	debris	above trend

There is some evidence, in the topographic data for the regions of the crater flows, of local uphill motion and surmounting of obstacles. Although the resolution of the topography is very poor for small-scale analyses, and thus this observation is uncertain, such behavior is consistent with the pyroclastic-type and sturzstrom models, and inconsistent with melt rock flow models. The presence of small shield volcanoes with 50 to 100 m relief which are not overtopped by the deposit (Figure 1*a*), however, implies a very low, uninflated character during flow. Inflated behavior would clearly be expected of nuée ardente-style pyroclastic flows, and perhaps of fireball containment flow as well (at least before vapor melt phase separation). The appearance of these domes in some flows, then, favors the sturzstrom-type debris model or the melt flow models for these flows. It seems inconsistent for sturzstroms to flow up slopes but not bury obstacles of equal or lesser height, but both behaviors are consistent with observations or terrestrial examples [*Hsü*, 1985]. The flow only goes up a topographic obstacle if it cannot flow around it: thus the Elm flow in Switzerland climbed the walls of a valley, but it enveloped a man up to the neck without burying (or crushing) him.

CONCLUSIONS

The outflow features associated with impact crater ejecta on Venus are very diverse. Some are apparently channel-like and erosive in nature, with streamlined islands and a large drainage region (Figure 13). Most, however, are apparently depositional in nature. Some deposits are very broad and poorly organized, with little structure apparent in radar imagery, while others are well channelized, with clear margins or levees. The depositional flows studied herein display a variety of source region and downflow morphologies, as well as diverse relationships to topography. Modelling the rheological properties of the flows results in a broad range of yield strength and Bingham viscosity estimates and in downstream trends in these parameters. It would probably be misleading to seek a single explanation for all these deposits. There is, in fact, evidence for at least two different processes:

1. One process follows emplacement of the ejecta and modifies the continuous ejecta blanket. This process is most likely to involve segregation of a basaltic melt fraction from the ejecta itself. Debris flow scenarios are not excluded, however, as the ejecta are emplaced with substantial momentum and internal energy. The processes of ballistic sedimentation, slope failure, and acoustic fluidization may combine to initiate mass movements and lengthy outflows.

2. A depositional process preceding ejecta emplacement, and stratigraphically underlying the ejecta blanket, must be associated with early stages of the impact event (jetting and vapor cloud), which expel basaltic magma, fluidized solid debris, or most likely a mixture of molten, solid, and vaporized debris, whose movement beyond about 0.5 crater radii past the rim is primarily controlled by topography but which may have the capacity to flow upwards for short distances. It is not highly inflated during flow. The very wide range in derived rheological parameters may indicate that a flexible model (in which the relative proportions of melt, solid, and vapor, as well as the composition of the melt and the size distribution of the solid fragments may all be varied) is probably the most useful framework for understanding crater outflow deposits. Its behavior may combine elements of pyroclastic flow, dry avalanche, and melt rock flow.

A satisfactory explanation of the existence of extended crater flow deposits on Venus requires a corollary explanation of their absence on other planets except perhaps for Earth, whose record is rapidly obscured. Such an explanation is available for both melt rock flow and debris flow hypotheses, respectively: (1) rates of impact melt production are higher on Venus due to higher surface temperature and impact velocity, and melt separation processes are more efficient due to higher surface temperature and pressure and larger ejecta particle sizes; and (2) interaction with a dense atmosphere is required to contain the vapor cloud in a ground-hugging turbidity flow. Both these explanations are subject to further experimental and theoretical testing.

Acknowledgments. The authors wish to thank Brennan Klose, Akihiko Hasimoto, Beth Holmberg, Craig Leff, and Peter Schultz for discussions and technical help. We are indebted to Phillip Shaller and Robert Herrick for providing unpublished data. This work was supported by JPL contract 958593.

REFERENCES

Bagnold, R.A., *The Physics of Blown Sand and Desert Dunes*, Methuen, London, 1954.

Baker, V.R., G. Komatsu, V.C. Gulick, and T.J. Parker, Channels on Venus: An overview, *Lunar Planet. Sci., XXII*, 45-46, 1991.

Basaltic Volcanism Study Project, *Basaltic Volcanism on the Terrestrial Planets*, Pergamon, New York, 1981.

Basilevsky, A.T., Cleopatra crater on Venus: Happy solution of the volcanic vs. impact crater controversy, *Lunar Planet. Sci., XXII*, 59-60, 1991.

Beget, J.E., and A.J. Limke, Two-dimensional kinematic and rheological modeling of the 1912 pyroclastic flow, Katmai, Alaska, *Bull. Volcanol., 50*, 148-160, 1988.

Bingham, E.C., *Fluidity and Plasticity*, McGraw-Hill, New York, 1922.

Cattermole, P., Sequence, Rheological Properties, and Effusion Rates of Volcanic Flows at Alba Patera, Mars, *Proc. Lunar Planet. Sci. Conf. 17th*, Part 2, *J. Geophys. Res.*, *92*, suppl., E553-E560, 1987.

Davies, D.K., M.W. Quearry, and S.B. Bonis, Glowing avalanches from the 1974 eruption of the Volcano Fuego, Guatemala, *Geol. Soc. Am. Bull., 89*, 369-384, 1978.

Eppler, D.B., J.H. Fink, and R. Fletcher, Rheologic properties and kinematics of emplacement of the Chaos Jumbles rockfall avalanche, Lassen Volcanic National Park, California, *J. Geophys. Res., 92*, 3623-3633, 1987.

Fink, J.H., and J.R. Zimbelman, Rheology of the 1983 Royal Gardens basalt flows, Kilauea Volcano, Hawaii, *Bull. Volcanol., 48*, 87-96, 1986.

Fink, J.H., M.C. Malin, R.E. D'Alli, and R. Greeley, Rheological properties of mudflows associated with the spring 1980 eruptions of Mount St. Helens volcano, Washington, *Geophys. Res. Lett., 8*, 43-46, 1981.

Glasstone, S., and P.J. Dolan, *The Effects of Nuclear Weapons*, U.S. Government Printing Office, Washington D.C., 1977.

Head, J.W., III, and L. Wilson, Volcanic processes and landforms on Venus: Theory, predictions, and observations, *J. Geophys. Res., 91*, 9407-9446, 1986.

Hulme, G., The interpretation of lava flow morphology, *Geophys. J. R. Astron. Soc., 39*, 361-383, 1974.

Hulme, G., The determination of the rheological properties and effusion rate of an Olympus Mons lava, *Icarus*, *27*, 207-213, 1976.

Hsü, K.J., Catastrophic debris streams (sturzstroms) generated by rockfalls, *Geol. Soc. Am. Bull., 86*, 129-140, 1975.

Johnson, A.M., *Physical Processes in Geology*, Freeman, Cooper, San Francisco, 1970.

Johnson, A.M and J.R. Rodine, Debris Flows, in *Slope Instability*, edited by D. Brunsden and D.B. Prior, pp. 257-362, John Wiley, New York, 1984.

Kargel, J.S., G. Komatsu, V.R. Baker, J.S. Lewis, and R.G. Strom, Compositional constraints on outflow channel-forming lavas on Venus, *Lunar Planet. Sci., XXII*, 685-686, 1991.

Komatsu, G., J.S. Kargel, V.R. Baker, J.S. Lewis, and R.G. Strom, Fluidized impact ejecta and associated impact melt channels on Venus, *Lunar Planet. Sci., XXII*, 741-742, 1991.

Limke, A.J., and J.E. Beget, Emplacement velocities and rheological properties of pyroclastic flows during the March 27-APril 8 eruption of Mt. St. Augustine, Alaska, *Eos Trans. AGU*, *67*, 1259, 1986.

McBirney, A.R., and T. Murase, Rheological properties of magmas, *Ann. Rev. Earth Planet. Sci.*, *12*, 337-57, 1984.

Melosh, H.J., Acoustic fluidization: A new geologic process? *J. Geophys. Res.*, *84*, 7513-7520, 1979.

Melosh, H.J., The mechanics of large rock avalanches, in *Debris Flows/Avalanches: Process, Recognition, and Mitigation*, edited by J.E. Costa and G.F. Wieczorek, pp. 41-50 Geological Society of America, Boulder, Colo., 1987.

Melosh, H.J., *Impact Cratering: A Geologic Process*, Oxford University Press, New York, 1988.

Moore, H.J., Preliminary estimates of the rheological properties of 1984 Mauna Loa lava, *U.S. Geol. Surv. Prof. Pap.*, *1350*, 1569-1588, 1987.

Moore, H.J., D.W.G. Arthur, and G. G. Schaber, Yield strengths of flows on the Earth, Mars, and Moon, *Proc. Lunar Planet. Sci., IX*, 3351-3378, 1978.

Murase, T., and A.R. McBirney, Properties of some common igneous rocks and their melts at high temperatures, *Geol. Soc. Am. Bull.*, *84*, 3563-3592, 1973.

Pettengill, G.H., P.G. Ford, W.T.K. Johnson, R.K. Raney, and L.A. Soderblom, Magellan: Radar performance and data products, *Science*, *252*, 260-265, 1991.

Phillips, R.J., R. E. Arvidson, J. M. Boyce, D. B. Campbell, J. E. Guest, G.G. Schaber, and L. A. Soderblom, Venus impact craters: implications for atmospheric and resurfacing processes from Magellan observations, *Lunar Planet. Sci., XXII*, 1063-1064, 1991.

Pierson, T.C., and J.E. Costa, A rheologic classification of subaerial sediment-water flows, in *Debris Flows/Avalanches: Process, Recognition, and Mitigation*, edited by J.E. Costa and G.F. Wieczorek, pp. 1-12, Geological Society of America, Boulder, Colo., 1987.

Ryan, M.P. and J.Y.K. Blevins, The viscosity of synthetic and natural silicate melts and glasses at high temperatures and 1 Bar (10^5 pascals) pressure and at higher pressures, *U.S. Geol. Surv. Bull.*, *1764*, 1987.

Schaber, G.G., Lava Flows in Mare Imbrium: Geologic evaluation from Apollo orbital photography, *Proc. Lunar Sci. Conf. 4th*, pp. 73-92, 1973.

Schultz, P.H., Atmospheric effects on oblique impacts, *Lunar Planet. Sci., XXII*, 1191-1192, 1991 *a*.

Schultz, P.H., Styles of ejecta emplacement under atmospheric conditions, *Lunar Planet. Sci.*, *XXII*, 1193-1194, 1991 *b*.

Schultz, P.H., Impactor signatures on Venus, *Lunar Planet. Sci., XXIII*, 1231-1232, 1992.

Schultz, P.H. and D.E. Gault, Seismically induced modification of lunar surface features, *Proc. Lunar Sci. Conf. 6th*, 2845-2862, 1975.

Shaw, H. R., Rheology of basalt in the melting range, *J. Petrol.*, *10*, 510-535, 1969.

Shaw, H.R., T.L. Wright, D.L. Peck, and R. Okamura, The viscosity of basaltic magma: An analysis of field measurements in Makaopuhi Lava Lake, *Am. J. Sci.*, *266*, 225-264, 1968.

Sparks, R.S.J., and H. Pinkerton, Effect of degassing on rheology of basaltic lava, *Nature*, *276*, 385-386, 1978.

Whipple, K.X. and J.R. Zimbelman, Field constraints on remote observations of debris flows and lava flows, *Lunar Planet Sci.*, *XXII*, 1497-1498, 1991.

Wilson, L., and J.W. Head III, Morphology and rheology of pyroclastic flows and their deposits, and guidelines for future observations, in The 1980 Eruptions of Mt. St. Helens, Washington, *U.S. Geol. Surv. Prof. Pap.*, *1250*, 1981.

Wilson, L., and J.W. Head III, A comparison of volcanic eruption processes on Earth, Moon, Mars, Io, and Venus, *Nature*, *302*, 663-669, 1983.

Zimbelman, J.R., Estimates of rheologic properties for flows on the Martian volcano Ascraeus Mons, *Proc. Lunar Planet. Sci. Conf. 16th*, Part 1, *J. Geophys. Res.*, *90*, suppl., D157-D162, 1985.

P.D. Asimow, Division of Geological and Planetary Sciences 170-25, California Institute of Technology, Pasadena, CA 91125.

J.A. Wood, Smithsonian Astrophysical Observatory, 60 Garden Street, Cambridge, MA 02138.

(Received October 1, 1991;
revised April 27, 1992;
accepted April 28, 1992.)